12-2018

Thermal Mechanical Numerical Modeling of Friction Element Welding

Ankit Varma
Clemson University, ankitvarma1102@gmail.com

THERMAL-MECHANICAL NUMERICAL MODELING OF FRICITON ELEMENT WELDING

A Thesis
Presented to
the Graduate School of
Clemson University

In Partial Fulfillment
of the Requirements for the Degree
Master of Science
Mechanical Engineering

---

by
Ankit Varma
December 2018

Accepted by:
Dr. Xin Zhao, Committee Chair
Dr. Hongseok Choi
Dr. Huijuan Zhao
Dr. Laine Mears

ABSTRACT

With the objective of minimizing carbon footprint of vehicles, different organizations across the world are increasingly enforcing higher fuel efficiency targets for the automobile manufacturers. To improve the fuel economy while retaining or further improving the structural integrity, the automobile industry is vigorously shifting towards substituting conventional heavy materials like cast iron with new age materials such as aluminum alloys, steel alloys, etc. which are not only much lighter but also offer superior strength-to-weight ratio. Engineers use a mix of these new age materials with the aim of maximizing the benefits from each material. However, the utilization of such materials is currently limited in the industry as welding them using conventional methods such as resistance spot welding or fusion welding process, is plagued with inherent difficulties such as formation of brittle inter-metallic compounds, irreversible and adverse changes in the thermal and mechanical properties of the materials.

Dissimilar material joining is of critical importance in aiding the manufacturers realize the crucial objective of a safer and more fuel efficient vehicle. Friction element welding (FEW), a friction based joining process, has been proposed for joining highly dissimilar materials in minimal time and with low input energy. FEW process can join a variety of materials which differ significantly in their mechanical, thermal, and metallurgical properties without inducing any of the defects associated with conventional welding methods. The fundamental governing mechanisms that characterize the FEW process needs to be investigated to help optimize the process for specific applications. Conducting experimental investigation is undesirable and infeasible due to the highly

complex thermal-mechanical procedures occurring simultaneously in a very short period of time of about one second. As such, the utilization of a finite element model to simulate and analyze the FEW process is warranted which would help understand the underlying mechanisms of the process in detail and provide an efficient yet effective tool to observe the effect of different process parameters on the weld quality.

A coupled thermal-mechanical finite element model (FEM) is developed in this work to simulate the FEW process and gain an understanding of the physical mechanisms involved in the process and help predict the influence of variation of process parameters on the evolution of temperature, material flow, and their effect on weld quality. The primary difficulty in simulating a highly transient process like FEW, wherein not only the workpiece is subjected to deformation but also the auxiliary joining element i.e. friction element undergoes extensive deformation, is that the mesh elements are prone to distortion failure while trying to capture such high amount of deformation. The presence and importance of temperature effect on material properties further complicate the FEM. To help eliminate the distortion issue while simultaneously achieving an accurate simulation of the FEW process, the coupled Eulerian-Lagrangian (CEL) approach is adopted. The novelty of the current approach employed lies in using a Eulerian definition for the tool as against the more traditional convention of adopting a purely Lagrangian definition. The Eulerian definition enables to simulate the extreme deformation of friction element and capture the material flow without any computational issues.

To inspect for the accuracy of the FEM results, mechanical deformation for different parts observed in the FEM is compared against the experimental results. To further

validate the FEM, experimental measurements of temperature at different locations at the interface of two layers of workpiece are compared against the FEM results at same locations in the model. With respect to, both, thermal and mechanical measurements comparisons good agreement is shown between the simulation results and the experimental data. The simulation results for sets with varying process parameters show that the rotational speed of the friction element has the highest influence on the amount of frictional heat generated followed by the time period for different steps. Higher amount of heat is generated and conducted into the top aluminum layer for longer Penetration time, whereas for more heat concentration into the friction element to achieve the required deformation, longer Welding step with higher rotational speed is desired.

DEDICATION

To y’all.

ACKNOWLEDGEMENT

I would like to express sincere gratitude towards my advisor Dr. Xin Zhao for reposing his faith in me in completing this difficult task and providing exceptional guidance and support throughout Master's thesis work. I would also like to thank the committee members for devoting time and providing valuable feedback to make this thesis a more proficient and useful one.

Nothing is possible without the much required support of family & friends. A heartfelt gratitude to all of them.

I would like to thank Honda R&D, Americas for providing essential information, experimentation resources, and computing resources to complete my research work.

I would like to thank the Clemson University for providing generous compute time on the Palmetto HPC.

I would also like to mention a special thanks to the staff at Mechanical Engineering department and the inter-library loan division of Clemson University libraries for working tirelessly with the sole aim of aiding students realize their goals.

Lastly, I would like to express my gratitude towards my spiritual guru Shri Swami Hari Prakash ji Maharaj for guiding me through the maze of life.

TABLE OF CONTENTS

Table of Contents (Continued)

LIST OF FIGURES

List of Figures (Continued)

LIST OF TABLES

CHAPTER ONE
INTRODUCTION

A material can be effectively utilized only if it has been given an end-user, consumer or manufacturer, based proper profile to facilitate its effective application and subsequent efficient disposal, absence of which a material is nothing but just worthless mass of substance. Materials are given this much required meaningful form by means of different manufacturing operations such as casting, forming, machining, grinding, welding, brazing, adhesive joining and more, depending on the product requirements. Among all these processes, the welding process is used extensively in varied forms in almost all production related operations across various industries, for example: automotive sector, aerospace sector, light/heavy industrial sectors, construction industry, food packaging, etc. More or less all the industrial user products and also almost all infrastructure projects make use of welding process in some or other form to make a product functional in daily life or to build something which is used for subsequent manufacturing of goods. Without these manufacturing processes, it would not be possible to utilize the materials to their maximum efficiency.

The process of welding is used to join two or more different parts together which may be made up of similar or dissimilar materials, in order to provide the required shape, strength, durability, etc. According to the American Welding Society (AWS), welding is defined as “A joining process that produces coalescence of materials by heating them to the welding temperature, with or without the application of pressure or by application of

pressure alone, and with or without the use of filler material". The oldest form of welding known is forging wherein the material is heated to plasticize it and then pressure is applied to shape a new product and induce strength in it. The process of welding has undergone tremendous transformation in the past several decades to better meet the prevailing requirements of an industry and is currently utilized in multiple forms, subject to the production requirements. Numerous variations of welding have been developed owing to the continuous development of new materials, economic considerations, environmental regulations, and precision products requiring state-of-the-art joining techniques. The diversification and modification of welding processes is a relentless procedure required to fulfil the present day demands of, both, the consumer and the producer.

The process of welding stands out against other joining techniques as it offers simple yet significant advantages such as ease-of-usage and handling, mobility of equipment, less skill and knowledge required compared to other processes such as machining, grinding, etc., the cost of process is relatively low, complete automation of welding process is possible in joining of various products thereby augmenting cost and time related savings. Several other methods are available for joining of different parts such as use of adhesives, soldering, brazing, riveting, etc. but none of them can be applied universally across industries for a diverse group of materials and also the required strength of the joined product is not met with these processes unlike in the case of welding.

1.1. Different Welding Methods Available in Automotive Industry:

The aim of the current thesis is to analyze a novel welding process for employing it in the automotive industry and as such welding processes pertaining to the automotive industry only shall be discussed here. Currently, there are numerous techniques which are prevalent in the automotive industry for joining two different parts and their application depends on factors such as sheet thickness, material properties, degree of precision required, strength of weld, production time, economic factors, ease of accessibility of parts to be welded, etc. Depending on these factors, an appropriate welding process is selected which satisfies the required criterion. Some of the more common welding processes employed in joining the materials are described next.

1.1.1. Fusion Welding:

In fusion based welding process, weld is obtained by heating the materials above their melting temperatures which allows efficient mixing of the molten materials in the weld region. Commonly, external filler material is added to the molten metal pool to fill any voids in the weld region to prevent any defect, strengthen the weld, and prevent formation of any undesirable compounds in the weld region. Filler material can be either same as the weld material or different from it. The presence of such high temperatures in the process results in the undesirable effect of irreversible changes in the mechanical and metallurgical properties of the weld materials. Fusion welding is one of the most ubiquitous and widely used process owing to the simple yet effective mechanism involved in welding

two parts together. Some of the widely used fusion based welding processes are gas metal arc welding (GMAW) [1], gas Tungsten arc welding (GTAW), plasma arc welding (PAW), resistance welding, laser welding, and electron beam welding (EBW). Processes such as GMAW/GTAW/PAW are characterized by heating of the material well above their melting point, low productivity i.e. high time consuming process[2], expensive equipment, requirement of skilled labor, etc. which makes them less favorable for application in joining of sheets of dissimilar materials. Resistance welding is the preferred process for joining sheet metals in the automotive industry due to its ability to produce strong welds between sheets of different materials in low time. The principle involved and the type of resistance welding used in automotive industry is discussed below.

1.1.1.1. *Resistance Welding*:

The fundamental principle involves passing high amperage, low voltage current[3] between the weld sheets via electrodes and as a consequence of resistance to the passage of current at multiple contacting locations, a large amount of heat is generated which melts the material in the contact region. At the end of the process, pressure is applied through the electrodes to form a solid mechanical joint between the two sheets. Variations of resistance welding includes, but not limited to, spot welding, seam welding, projection welding, butt welding, flash welding, and upset welding. Different resistance welding processes are used depending on the sheet thickness, materials to be welded, ease of access to weld material region etc. The resistance spot welding is extensively used in the automotive industry to join different sheet metal parts of varying thickness as it offers

advantages such as high efficiency, very low process time and high rate of production, absence of filler material, and can be made 100% autonomous. Due to localization of heat input it produces a very small heat-affected zone thereby minimizing the effect on mechanical properties of the weld material. Resistance welding is appropriate for materials that have low thermal conductivity, high resistance and low melting points, however for using it on materials which have high thermal conductivity such as aluminum based alloys the electrode material has to be modified accordingly to provide a higher heat input concentration to melt the material and subsequently produce the weld[1]. Welding processes such as laser beam welding or electron beam welding have not yet been fully developed with respect to utilizing them in a production line. Its utilization is also limited due to factors like high initial cost of equipment, energy intensive source, controlled environment for functioning of equipment[3], etc. They are used for special applications such as precision welding due to their ability to produce small diameter welds between very thin sheets, for materials which are not suitable to be joined by other processes, for sheet materials having high thickness, etc.

1.1.2. Solid State Welding*:*

In solid state welding process, the temperature of the weld materials undergoing joining process remains below the melting temperature thereby inducing only plasticization and not melting, also no external filler material is required[4]. Pressure may or may not be applied on the plasticized region during the joining process to obtain a solid mechanical joint between the two parts. As the temperature in the process doesn't reach the solidus

point or in some cases it reaches the solidus point but only transiently, no significant detrimental changes are induced in the mechanical behavior of the weld materials[4] unlike in the case of fusion welding process where the mechanical characteristics of the weld materials undergo irreversible changes. Different solid state welding processes can be used for joining wide scale of similar or dissimilar materials with good efficiency. Some of the drawbacks associated with it are: tooling can be complicated, ease of inspecting the weld is low, repairing/modifying a process induced defect in the weld joint is highly difficult[2]. The different forms of solid state welding are friction welding, ultrasonic welding, pressure welding, and explosion welding. Among these solid state welding processes, friction welding is one of the most extensively used and also widely researched process owing to its simple joining mechanism[3], ability to weld a wide variety of highly dissimilar materials, etc. As a result of continuous research & development, varied forms of friction welding have come into existence. Some of the more popular forms of friction welding are

- *Friction stir welding*, an external tool is given rotational feed and pressed against the workpiece to be welded resulting in friction heat generation and as the tool translates through the welding region a joint is formed between the parts due to the plasticization and stirring (mixing) of the weld materials.
- *Friction stir spot welding,* it is very much similar to friction stir welding with the primary difference being that it used for making lap joints (like spot welds) and it does not involve lateral movement of the tool.

1.2. Current Trend in Automotive Industry:

The primary aim of any engineer, be it in automotive industry, aerospace industry or any other manufacturing oriented industry, is to minimize the weight of the product without compromising the performance characteristics of the product. Many of the North American automotive original equipment manufacturers (OEMs) have made an objective to strive for vehicle weight reduction by 350 kg i.e. to reduce the weight of the vehicle by 20% by the year 2020[5] and this phenomenon is more popularly known as the process of "lightweighting". The critical aim of weight reduction is fueled by many factors such as stringent environmental norms aimed at reducing carbon emissions, achieving superior and efficient product performance, cost competition in the market, increasing product reliability, etc. and this aim is viable only by utilizing modern materials and their alloys which have excellent mechanical, thermal, and metallurgical characteristics, for example high strength alloys of aluminum, steel, composite alloys, metal matrix composites, and so on which not only offer improved mechanical strength but are also lightweight. According to [6], aluminum alloys offer a strength-to-weight ratio to the order of 3:1 when compared against the steel alloys which implies that in case of a similar body (or part) design, aluminum alloys will weigh up to 70% less than their steel alloys counterpart. Isenstadt et al. [7] has provided a review of the trend in weight reduction of vehicles with respect to the factors driving this trend, progress achieved, penetration of this phenomena in the USA automotive industry, cost benefits achieved from it, etc. There has been an aggressive push towards lightweighting of the automobiles by substituting the conventional materials, cast iron and steel, with the lightweight materials which can result in weight reduction as high

as 50%[8]. According to [9], a reduction of about 100 kg in a vehicle decreases the fuel consumption from 0.3-0.5 liters per 100 km and as per [10], a 10% reduction of weight in a mid-size family car which weighs about 1,450 kg can result in 6-8% improvement in fuel consumption with the usage of lightweight materials. Several commercial passenger vehicle manufacturers are increasingly adopting lightweighting strategy, an example of this can be seen in FIGURE 1 where General Motors have significantly reduced the weight of their current fleet of vehicles. More recently, Chrysler was able to achieve a weight reduction of around 60 kg in the body-in-white structure of their passenger vehicle 'Pacifica' (refer FIGURE 2) by utilizing different lightweight materials[11]. According to [12], Ford has utilized an aluminum intensive based body and cargo box in their vehicle 'F-150' whereas Audi achieved a body weight reduction of 40% in their vehicle 'A8' by extensively using aluminum alloys[13].

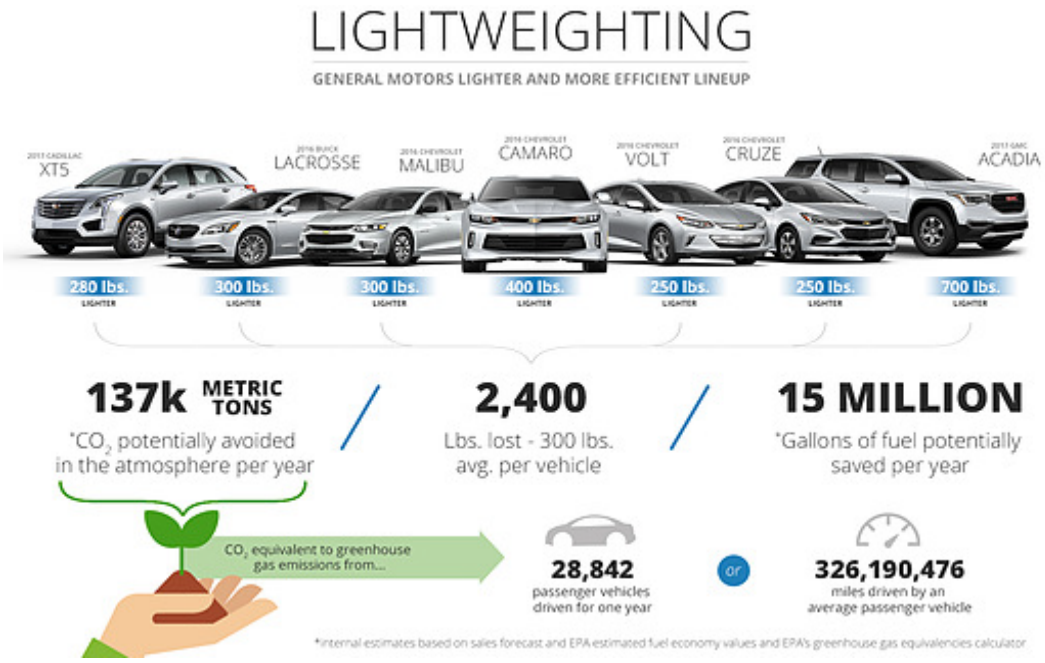

FIGURE 1 LIGHTWEIGHTING OF VEHICLES BY GENERAL MOTORS [14]

FIGURE 2 BODY-IN-WHITE STRUCTURE OF CHRYSLER PACIFICA[11]

1.3. Welding of Dissimilar Materials in Automotive Industry:

The new-age materials which possess superior mechanical properties are inundated with their own problems due to the significant differences in their metallurgical and physical properties of these materials. Many of these materials cannot be efficiently joined/cut/machined using the conventional processing operations and requires special operating tools/machinery and processes which can work on them without degrading their performance characteristics. The importance of developing methods for joining dissimilar materials in the automotive industry can be gauged by the fact that major automobile manufacturing companies are aiming towards replacement of conventional materials with lightweight materials such as aluminum alloys, steel alloys, metal matrix composites, etc. which provide better strength to weight ratio [refer FIGURE 3]. Although the light weight

alloys offer various advantages which makes them beneficial to utilize in the product, their realization in the designed product is limited due to various factors such as: conventional joining processes cannot be used for these materials as it might alter their physical (mechanical & thermal) characteristics and in some cases cause irreversible transformation of microstructure thereby rendering them less effective. Joining of two or more dissimilar alloys can be accomplished only if the materials have coherence towards each other and form a strong bond at the atomic level i.e. materials with greatly varying properties such as thermal conductivity or melting temperature cannot be easily welded making it difficult to find a process with parameters suitable for both materials[15], and the process time can be too long which is undesirable if it has to be introduced in the production line.

An example of using different construction materials for motor vehicle body components: 1 – magnesium alloys; 2 – aluminium alloys; 3 – low-carbon deep-drawing steels; 4 – higher-strength steels HSS; 5 – high-strength steels; 6 – very high-strength steels; 7 – ultrahigh-strength steels

FIGURE 3 APPLICATION OF LIGHTWEIGHT MATERIALS IN AUTOMOBILE[16]

Some of the joining technologies prevailing in the automotive industry are discussed below.

1.3.1. Resistance Spot Welding:

According to [6], there can be as many as 6000 spot welds in a single automobile, signifying the heavy reliance on this joining technique by the manufacturers. Spot welding offers unique advantages of low cost, low process time, and universal applicability on several materials but employing resistance spot welding for materials like aluminum alloys, steel alloys, etc. is not feasible because the process requirements of these materials makes it difficult to weld them together using spot welding, for example due to high thermal conductivity of aluminum it requires unusually high current input which affect the electrode life cycle[17]. Progress has been made in employing spot welding for dissimilar materials by modifying the process parameters and also by introducing external elements which aids in the joining process.

1.3.2. Friction Welding:

Friction based welding processes are principally solid state joining process and it's employed across many industries such as aerospace, marine, automotive, railways, etc. There are several variations of friction welding currently in use in the automotive industry for joining dissimilar materials, of which some of the main processes are friction stir welding, friction stir spot welding, linear friction welding, friction stir forming, friction bit joining and so on. Friction based welding process have been used for welding aluminum alloys to steel alloys[15,18] as well as aluminum to thermoplastics[19]. Of the many friction based welding processes, friction stir welding has gained significant attention for joining materials of varying thicknesses and incompatible physical/metallurgical properties

due to the various benefits it offers in the form of: no pre or post processing requirement, a non-consumable tool is used which helps in non-addition of weight to the structure, no hazardous waste or fume or requirement of filler material as compared to arc welding process, and ability to join dissimilar materials[20,21]. Despite these advantages, its application is fairly low when compared with resistance spot welding due to certain drawbacks such as need to access both sides of materials being joined, requirement of applying high load on the tool to maintain the alignment and generate heat which necessitates the use of heavy welding equipment to support the workpiece, formation of a hole at the end of joint when the tool is retracted, long processing time which prevents it to be applied in mass production environment, tool material is required to be of higher strength than parent weld materials to avoid wear, and in case of excessive tool wear the weld quality can be severely affected. A brief comparison between friction based welding processes and conventional joining processes is described in TABLE 1.

TABLE 1 COMPARISON OF FRICTION WELDING AND CONVENTIONAL WELDING PROCESS

Friction based welding process	**Conventional welding process**
No change in the physical properties of the welded materials.	Irreversible changes in the physical properties of the welded materials due to the high temperature.
No weld defects such as slag inclusion, porosity, oxide formation, etc. are present.	Marked by the presence of weld defects if the welding parameters aren't controlled appropriately.
No requirement of filler material, flux, or any type of shielding gas.	Requires the use of filler material, shielding gas, etc. to obtain a satisfactory weld.
Can easily weld dissimilar materials together with little or no pre-processing.	Difficult to weld dissimilar materials together, possible only by a few processes such as EBW, LBW
Less-energy intensive. Environmentally friendly process.	High-energy intensive process with comparatively higher environmental costs involved.
Welding equipment portability is low, as such it requires to be fully automated	Welding equipment can be moved around relatively easy except in cases of EBW, LBW, PAW

Friction based welding process	Conventional welding process
In some friction welding processes such as linear or orbital or rotary friction welding, the application is limited due to geometry of the parts involved.	No limitation of using parts of particular geometry.
High precision or tolerances based weld joints are difficult to achieve.	With narrow concentrated heat source based process, it is possible to achieve precision weld joints.
Absence of fumes, post-process slag or use of chemicals makes it environmentally friendly.	Due to the fumes, oxides, and post-process products involved, it's relatively less environmentally friendly.

1.3.3. Mechanical Fasteners:

The application of mechanical fasteners in the automotive industry has been around for a long time in the form of screws, nuts and bolts, to the more advanced current form of flow drilling screws, clinching, different types of riveting. It is one of the oldest method of joining two metal parts together by using an external joining element i.e. 'fastener'. There are few variations of mechanical fastening process, although the primary principle in these variations is same i.e. piercing of the top layer which is placed in a lap configuration by the fastener wherein a hole might be pre-processed to facilitate its movement into the workpiece. Using mechanical fasteners offers advantages such as no requirement of pre-

processing (except in case of blind riveting), minimal effect of thickness on processing time[22], ease of joining dissimilar materials, easy removal in case of failure/deterioration without causing damage to the parent structure[23] and it is environmentally friendly. The limitations in employing this technique are: requirement of access to both sides of the materials being welded, fasteners tend to increase the overall weight of the product[22], it might result in stress concentration thereby affecting the strength of the joined product[1], requirement of ductile materials for process like clinching, and limitations on the thickness of the sheets that can be joined[21].

1.3.4. Adhesive Joining:

It involves forming a joint between two materials mainly positioned in a lap configuration by the use of adhesive which develops an intermolecular joint with the two parent metals under application of load[1]. It is also a solid-state joining process as it does not involve the fusion of any of the parts to be welded. Besides being a solid state process, its other salient features are: absence of distortion of materials due to fusion, provides a seal/leak proof joint, prevents augmentation of stress concentration as the adhesive joint is spread uniformly enabling improved fatigue life[23], dissimilar materials can be joined easily[22]. Adhesives have also been used in combination with spot welding to provide a seal proof joint. Its applicability for the new age materials is limited as the reliability of joint strength is only effective in a limited temperature range[1], the welded materials might require post-processing in the form of curing to strengthen the joint, use of fixtures to support the workpiece against the applied load[22], voids may occur in the joint in case

of uneven spreading of adhesive, and surface treatment might be required to achieve a reliable joint[21].

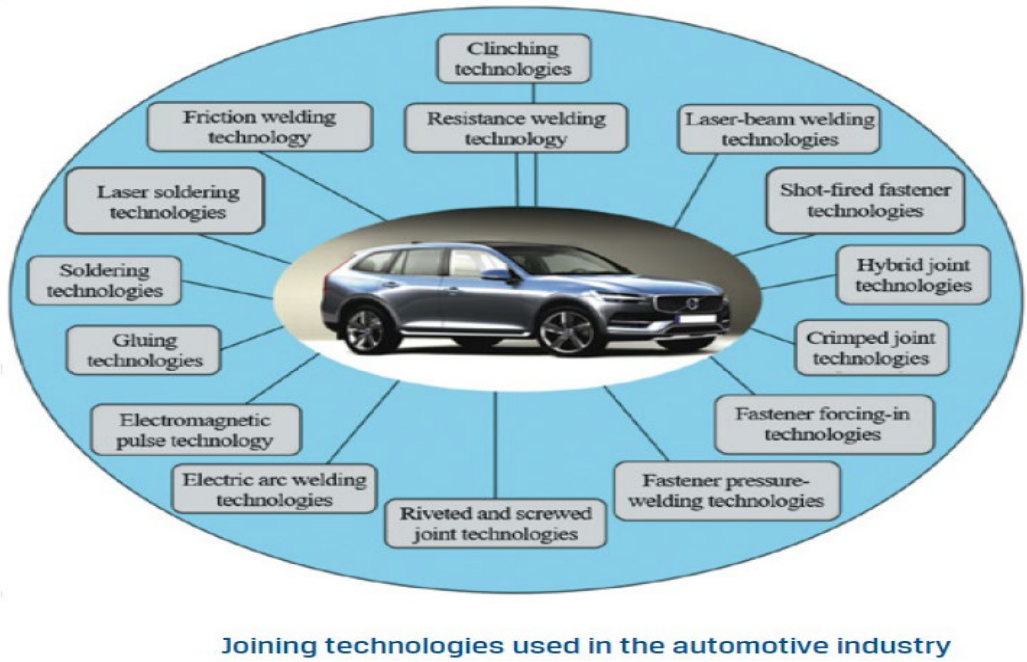

FIGURE 4 DIFFERENT WELDING METHODS EMPLOYED IN AUTOMOTIVE INDUSTRY[16]

1.4. Friction Element Welding:

For the period 2017-2025, the US Environmental Protection Agency (EPA) and the Department of Transportation's National Highway Traffic Safety Administration (NHTSA) has set guidelines to increase the average fuel economy from current 35.5 mpg to 54.5 mpg for passenger cars, light-duty trucks and medium-duty passenger vehicles which would result in reducing the greenhouse gas emission approximately by 2 billion metric tons. Apart from this, the 'Vehicle Technologies Program' under the Department of Energy has

aimed at a maximum weight reduction of 50% in vehicle body and chassis systems[24]. With the stringent environmental norms and ambitious weight reduction targets set by various governments and organizations across the world for the coming years for vehicles belonging to various categories, automobile manufacturers are looking towards using lightweight materials so as to produce vehicles which are in compliance with the latest environmental norms while also meeting the safety requirements. The limitations associated with joining of dissimilar materials as mentioned earlier can be overcome by the use of a solid state welding process which not only ensures a defect-free weld of good quality but can also weld wide range of materials which have highly dissimilar properties. Currently in the automotive industry there are a number of joining process which are utilized to satisfactorily join sheet metals of multiple materials, these include resistance spot welding, structural adhesives, self-piercing riveting, remote laser welding, flow drilling screws, and RIVTAC®. Hybrid welding such as ultrasonic spot welding has been utilized for welding dissimilar materials[25] to overcome the limitations of spot joining high strength sheet metals, different forms of friction stir spot welding which do not leave a key hole after the process is completed have been developed and are being analyzed for its feasibility in joining dissimilar materials[26,27], clinching process has also been utilized to join the sheet metals of varying thickness and of strength up to 700 MPa[28,29], self-piercing riveting is also another mechanical joining process which has been gaining traction to join sheet metals[30,31]. Clinching, self-piercing riveting, spot welding requires two-sided access of the sheet metals but in case of one sided access, the processes which can be made use of are Bölhoff's RIVTAC® and flow drill screws[32] to join the sheet

metals. Each of these processes have limitations in one form or other, for example resistance spot welding cannot efficiently be used for aluminum alloys and high strength steel alloys, friction stir spot welding is a long duration process and hence not suitable for employing it in a mass production environment, mechanical joining process such as SPR and clinching requires two sided access and can weld sheet metals of up to a certain tensile strength only[33], whereas the noise levels in RIVTAC process are very high and local deformation of joining spots has been observed[34].

EJOWELD® Friction Element Welding (FEW) is a process developed by EJOT GmbH[35] which aims at joining sheet parts of different materials, like high strength alloys of aluminum to advanced and/or ultra- high strength alloys of steel, with varying thicknesses by employing the principle of friction induced heat and plasticization of the workpiece material with the help of an external tool called 'friction element' which is consumed in the process and aids in forming a leak-proof joint. FEW process fabricates a lap joint between the sheet metals placed one above the other, wherein ductile alloys with thickness up to 5 mm can be used for the upper for top sheet whereas steels, with or without coatings, with tensile strength ranging from 270 MPa to 1600 MPa and thickness up to 2 mm can be utilized for the lower or bottom sheet material[33]. In some cases, to produce a leak proof joint adhesives might be used along with the friction element in the FEW process. The FEW process being a fully automated and low time consuming process, has the potential to replace the current sheet joining methods used in the automotive industry.

The friction element welding process is a simple yet robust process which is categorized by four steps: Penetration, Cleaning, Welding, and Compression as can be seen in FIGURE 6. An external part 'downholder' is utilized in the process which performs critical functions of ensuring proper alignment of the tool and also that the layers of sheet material are pressed against each other thereby avoiding a gap between them during the entire process.

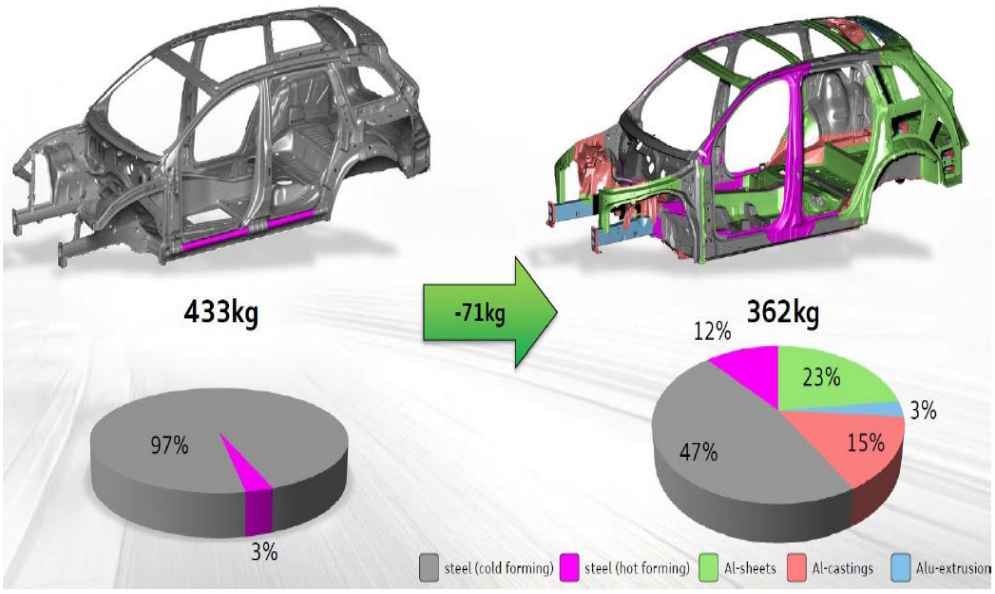

FIGURE 5 APPLICATION OF FEW PROCESS IN AUDI® Q7[35]

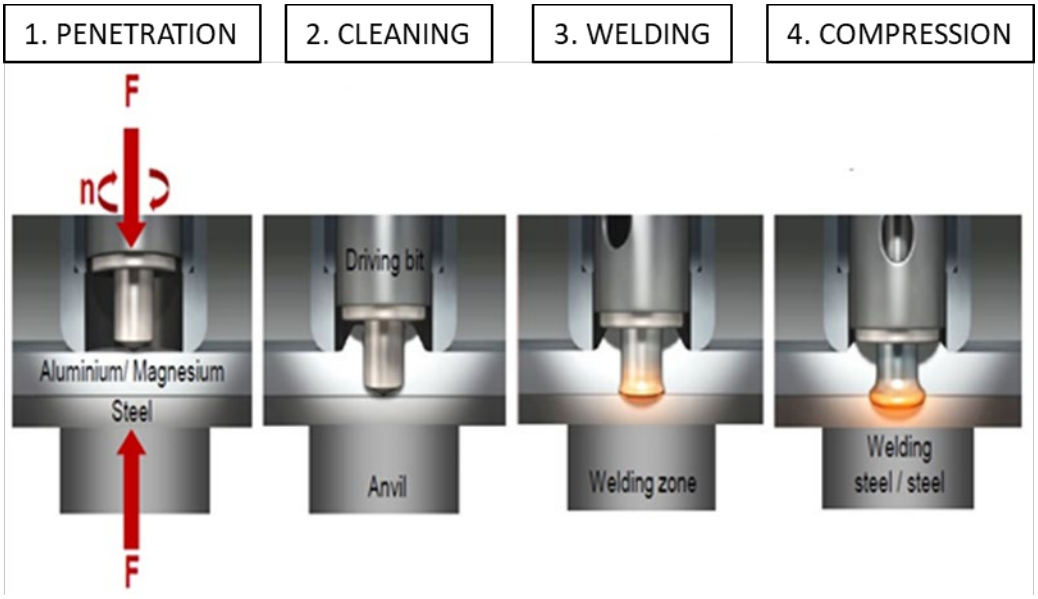

FIGURE 6 STEPS INVOLVED IN FEW PROCESS[35]

i. *Penetration:* In the first step, the consumable tool i.e. friction element is given a high rotational speed and pressed against the top sheet material under a constant load. The heat generated due to the interaction between the rotating tool and top sheet material induces plastic deformation in the latter thereby facilitating the movement of the element into the top sheet. The amount of heat generated and the distance travelled by the tool into the top sheet can be controlled by the rotational speed and load applied which primarily depends on the thickness and physical properties of the top sheet material.

ii. *Cleaning:* In the second step of FEW, the rotational speed of the friction element which has penetrated the top sheet is modified along with the external load applied on it. The friction element makes a through-hole in the top sheet and comes into contact with the bottom hard material and generates heat due to the friction interaction between them. This

interaction between element and bottom sheet has multiple effects of removing any layer of oxide or coating present on the bottom sheet as well as allowing sufficient heat generation in order to initiate the deformation of the friction element.

iii. *Welding:* In the third step, rotational speed and endload are modified as per requirements with the objective of raising the temperatures of friction element and bottom sheet to sufficiently high values which would induce plastic deformation in the contacting parts. As a result of elevated temperature, friction element experiences large amount of localized plastic deformation in its bottom region under the application of endload. The bottom sheet is also subjected to deformation, the extent of which depends on its material properties. The laterally deforming friction element displaces the top sheet to fill the gap present under the element shoulder head.

iv. *Compression:* In the final step, rotational feed is cut-off to the element and the endload is increased substantially to further deform the friction element and forge a bond between the element and two sheets of the workpiece. The top sheet material continues to fill the gap between itself and element shoulder head developing a mechanical interlock whereas the element develops a bond with the bottom sheet under the influence of high compression endload. The load to be applied in this step must be carefully monitored as excessive application of load can cause undesirable deformation of the friction element and it can penetrate deep into the bottom sheet.

The geometry and material choice for the friction element is dependent on the thickness and strength of the materials to be lap welded using FEW process. For any given set of two sheets, the strength of the friction element must compulsorily exceed that of greater strength of the two materials.

A brief comparison of different welding processes with respect to factors such as accessibility required, types of materials for which they can be used, requirement of additional joining parts, etc. have been provided in TABLE 2.

TABLE 2 COMPARISON OF DIFFERENT JOINING PROCESSES

Process	Accessibility required	Sheet Thickness Limitation	Eligible Materials	Processing Time	Weld Type	Dissimilar Materials Joining	Auxiliary Joining Part	Weight Added to Vehicle	Cost-effectiveness
Friction element welding	Two-sided	1 to 5 mm	AHSS, UHSS, Al alloys	0.9~1.2 s	Lap welds	Yes	Required/ Consumed	Yes	High initial tooling cost, element cost are limiting factors
Friction stir welding	One-sided	≥5 mm	Alloys of Al or Mg , HSS	> 10 s	Lap/ Butt welds	Yes	Not required	No	Stronger stir tools requirement make it less cost-effective
Friction stir spot welding	One-sided	1 to 2 mm	HSS, AHSS, Al alloys	> 2~5 s	Lap welds	Yes	Not required	No	Same as for friction stir welding
Friction-self piercing riveting	Two-sided	≤ 2 mm	AHSS, UHSS	1.5~3 s	Lap welds	Yes	Required /Consumed	Yes	Cost of rivets make it less competitive against RSW
Flow drill screws	One-sided	≤ 1 mm	HSS, Al alloys, AHSS	2~5 s	Lap welds	Yes	Required /Consumed	Yes	Relatively simple machine set-up & low strength screws make it cost effective
Friction bit joining	One-sided	1.5~2 mm	AHSS, UHSS, Al alloys	> 5 s	Lap welds	Yes	Required /Consumed	Yes	Additional cost of friction bits and initial investment make it less cost-effective against RSW
RIVTAC® screws	One-sided	1~4 mm	AHSS, UHSS, aluminum alloys	1~2 s	Lap welds	Yes	Required /Consumed	Yes	High initial tooling cost, joining screws cost make it less competitive against RSW
Resistance spot welding	Two-sided	1~2 mm	Conventional steel, aluminum alloys	1~2 s	Lap welds	Limited capability	Not required	No	Cost effective due to low tooling cost, non-requirement of auxiliary joining elements

1.5. Research Objective:

The primary objective of the research work conducted is to provide an efficient finite element model to analyze the different weld forming mechanisms occurring during the FEW process. With the help of developed FEM, it would be easier to understand how different output factors such as temperature, material deformation, and weld formation correspond to variations in the process parameters of endload, rotational speed, etc. The FEM would also enable to analyze the movement of different materials within the weld region which is not possible in experiments, and heat generation & distribution in different parts. For realizing this objective, a finite element model is developed using commercial software ABAQUS and its results will be validated against experimental observations.

CHAPTER TWO
LITERATURE REVIEW

2.1. Literature Review of Friction Based Joining Processes

Friction element welding is a new process due to which the amount of research work conducted on it is relatively less and as such there is lack of adequate literature pertaining to its finite element modeling except for some experimental work carried out in the industry domain[36] for analyzing its feasibility and comparing it against competing processes. With respect to finite element modeling of the FEW process, no literature could be found in the academic domain and therefore this review will be limited to processes which are fairly similar to the FEW process with respect to the joining mechanism, such as friction stir welding, friction stir spot welding, friction self-piercing riveting, etc.

Researchers have used different types of finite element modeling software and adopted a number of formulations i.e. pure Lagrangian, pure Eulerian, combination of Eulerian-Lagrangian, etc. depending on the requirements and available input information & computing resources to build the finite element model and examine the process. The finite element modeling of such mechanical joining processes comes with its own set of problems which require implementation of novel formulations, material response models, meshing strategy, proper interaction definition between different materials, etc. to successfully correlate the model with the experimental results and then further utilize it to understand the different mechanisms involved in the process. One of the main difficulties observed in developing a satisfactory FEM for highly transient process such as friction stir welding, friction drilling, flow drill screws, etc. is the problem of excessive distortion of

elements involved in the process, for which different techniques such as adaptive remeshing[37–39], damage failure for elements which removes the highly deformed elements based on a predefined criterion[40–42], or using Eulerian formulation of fixed mesh are being used[43–46]. Although, these techniques have been proven to avoid the distortion problem to a large extent, its usage results in high computational time and as such a fine balance has to be maintained between required degree of accuracy of a FEM and technical limitations like simulating extreme deformations, coupled behaviors, mesh density and distortion. The other major factor effecting the successful completion of numerical calculations is that of computing resources and the resulting compute time requirement for a given FEM. The computation time, depending on factors such as complexity of model, computing resources, etc., can vary from few hours to few months.

Schwer[47] performed a comparative analysis highlighting the features of different modeling schemes such as mesh free method, arbitrary Lagrangian-Eulerian (ALE) method, and Lagrangian method with element erosion whereas Lorrain et al.[48] analyzed different aspects such as constitutive laws determining material deformation, contact definitions between interacting parts, and application of mass scaling which are involved in building an FEM. Using a coupled thermal-mechanical FEM, processes such as friction stir welding, friction stir spot welding have been investigated for their material flow, temperature evolution, effect of tool profile, etc.[38,44,49–66]. With the purpose of avoiding mesh distortion due to extreme deformation, researchers are shifting from pure Lagrangian or pure Eulerian schemes to coupled Eulerian-Lagrangian (CEL) approach in which the tool is defined as Lagrangian object whose mesh is deformable while the

workpiece is modeled as Eulerian object having a fixed mesh to analyze the friction stir welding process[67–69]. Another popular method used for wholly eliminating the mesh distortion issue in the modeling of friction based joining processes is that of smoothed particle hydrodynamics (SPH)[51,70–75] wherein the elements are replaced by independent particles and the density of particles determine the accuracy of results as well as the computation time. Some researchers have also made use of 2-dimensional and/or axisymmetric modeling schemes instead of regular 3-dimensional modeling to simplify the FEM to drastically reducing the total computation time from days to hours without reducing the accuracy of the results[76–79]. Arbitrary Lagrangian-Eulerian (ALE) scheme has also been used to minimize or completely remove the mesh distortion issue when simulating highly transient processes such as friction stir spot welding[80,81].

More recently, emphasis has been laid on mechanical joining techniques for sheet metals such as clinching, friction self-piercing rivets, flow drill screws, etc. [82]. Different commercial software such as ABAQUS, ANSYS, FORGE, LS-DYNA etc. have been used by researchers to simulate clinching[83,84], self-piercing riveting (SPR)[85–90], flow drilling screws[42,91], friction-SPR[87,92].

In most existing models for other joining techniques, the tool undergoes relatively small amount of deformation when compared with the deformation of workpiece and as such it is generally considered as a rigid body to simplify the FEM. However, in the FEW process, the tool is subjected to severe localized plastic deformation, which is an essential factor for the final joint quality evaluation. Therefore, the rigid tool assumption is not valid here, and it is important and challenging to predict the tool deformation and material flow

as well. Besides the deformation, the inter-dependency of mechanical and thermal properties further complicates the model and have an adverse effect on the computation time.

With such inherent limitations and the remedial measures available to subdue them, a coupled thermal-mechanical FEM of the FEW process will be developed using ABAQUS software with the intent of studying the joining mechanisms and the response of the model to variation in process parameters. The modeling strategy adopted and the key features & difficulties involved are discussed in the next section for providing a reference to the reader to better understand the finite element procedure and the associated possibilities of simulating such processes.

CHAPTER THREE
FINITE ELEMENT MODELING

3.1. Finite Element Modeling of Friction Element Welding:

Experimentally, it is extremely difficult to understand the different mechanisms at play during the joining process as the experimental set-up hinders visual or any other kind of meaningful observation of the process. The finite element model to simulate the FEW process serves the purpose of revealing the underlying physical mechanisms involved in the process to help make it efficient with respect to different requirements. The FEW process is a highly transient process in which not only the workpiece material but also the tool (friction element) material undergoes significant deformation. Besides, the material properties vary in accordance with prevailing temperature during the joining process which requires the FEM to be thermo-mechanically coupled so as to achieve a realistic simulation of the joining process. During the FEW process, the friction element and the top layer of workpiece are subjected to extreme deformation, which means that the finite elements of these entities are poised to distort severely which can ultimately result in immature ending of the FEM calculations. There are a number of remedial measures which have been adopted by researchers to overcome the element distortion problem such as using remeshing technique at high frequency, deleting highly deformed elements based on some specified damage failure criteria, or using Eulerian elements which are not prone to distortion. The choice of the technique to prevent element distortion is a highly subjective one and requires critical assessment of effect of the chosen technique on the results of FEM. It is important to note that the primary difference between simulating FEW process and

other similar mechanical joining process involving application of friction based heat is that friction element in FEW process is not only consumed but also subjected to deformation. In the finite element modeling of all other mechanical joining processes such as friction stir welding, friction stir spot welding, RIVTAC, clinching, etc. the tool is considered as a rigid body as it experiences relatively small amount of deformation as compared with the workpiece materials, thereby simplifying the FEM process to a considerable extent and saving computational time.

The FEM of FEW process was developed using ABAQUS software due to the versatility of modeling approaches, in-built features to handle element distortion, ability to solve thermo-mechanical coupled equations in a reasonable amount of computational time, and availability of a range of material models for modeling the elastic-plastic behavior as well as defining the element deletion criterion. In ABAQUS/CAE, there are multiple schemes available to help cope with element distortion and deletion issues and many of them were investigated for their computational efficiency for modeling the FEW process. The options examined include Arbitrary Lagrangian-Eulerian (ALE) meshing, pure Lagrangian scheme with element deletion method, using mass scaling in regions experiencing large deformations with varying degree of scaling for different steps, combination of mass scaling feature and ALE meshing, and lastly, coupled Eulerian-Lagrangian (CEL) scheme. Selection of the appropriate scheme is critical to achieve a realistic simulation of the FEW process which would provide accurate results to help understand the bond formation, predict the influence of process parameters on the outputs and weld quality. Coupled Eulerian-Lagrangian (CEL) approach has been adopted in this

work to simulate the FEW process wherein the friction element is defined as a Eulerian entity and the two layers of workpiece are defined as Lagrangian entities. The Eulerian nature of the friction element allows the material to freely expand against the workpiece under the application of load without subjecting the elements to deformation and therefore, removing any possibility of distortion. The friction element was modeled as a Eulerian object only after thorough consideration and running multiple simulations in which it was defined as an Lagrangian object was unable to capture the required deformation in the process [refer FIGURE 7].

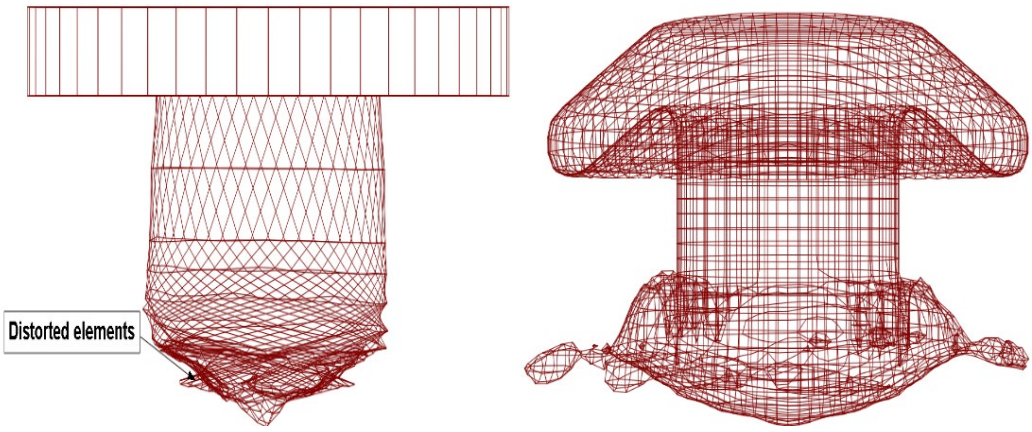

FIGURE 7 DEFORMED FRICTION ELEMENT,

LAGRANGIAN MESH (LEFT), EULERIAN MESH (RIGHT)

The dimensions of the Eulerian mesh domain which encloses the friction element are chosen such that no material is lost in the simulation. Too large of a domain would make it computationally unfeasible while too small of a domain would not be sufficient to

capture the entire deformation of friction element and also lead to material being lost in the simulation. With the objective of minimizing the computational cost, different Eulerian domain sizes were tested and the minimum size which proved to be efficient was selected (refer FIGURE 8). The Eulerian Volume Fraction (EVF) for the complex shape of the friction element is generated inside the Eulerian domain using the reference geometry of friction element. The geometry of the friction element and workpiece is shown in FIGURE 9. The two layers of the workpiece (first layer: Al 6061 T6; second layer: JSC 980Y and SAE 1008) are circular in shape with a radius of 8.1 mm out of which 5.4 mm radius is defined as deformable region (blue colored region in FIGURES 10 & 11) while the region towards the outer edges measuring 2.7 mm in radius is defined as rigid region (red colored region in FIGURES 10 & 11). The purpose behind defining deformable and rigid regions within a layer is two-fold, firstly it helps in reducing the computational cost by removing the elements from computation which do not experience noticeable amount of deformation and secondly, it aids in keeping the two layers in contact throughout the process with the use of 'sticking' contact condition between them. The second objective is more important because motion is specified to the workpiece layers instead of the tool, the reason for which is discussed in the boundary conditions & loads section. Based on the experimental results, a radius of 5.7 mm was chosen for the deformable region which is adequate to capture the material flow of the top layer without having any adverse effects on the FEM results. Two different materials were used for the bottom layer, SAE 1008 alloy was used for FEM validation against experimental results whereas JSC 980Y was used to evaluate the effect of process parameters on model outputs. The friction element material is SAE 4340, with

a radius of 2.275 mm and a length of 5.5 mm (not including shoulder). All the thermal and mechanical properties used for different parts are temperature dependent to ensure a true representative simulation of the process.

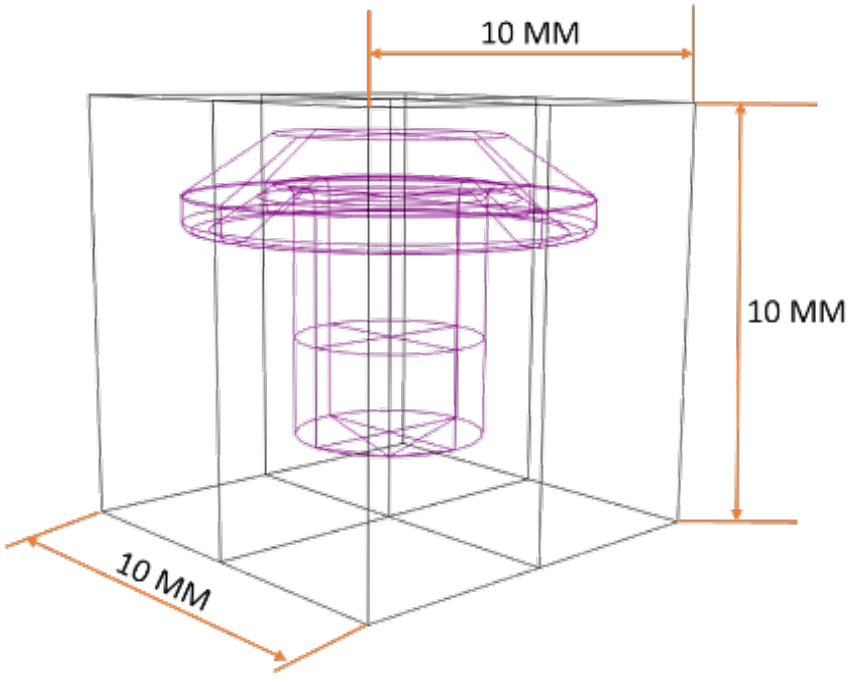

FIGURE 8 EULERIAN MESH DOMAIN DIMENSIONS WITH REFERENCE LAGRANGIAN FRICITON ELEMENT IN THE INTERIOR

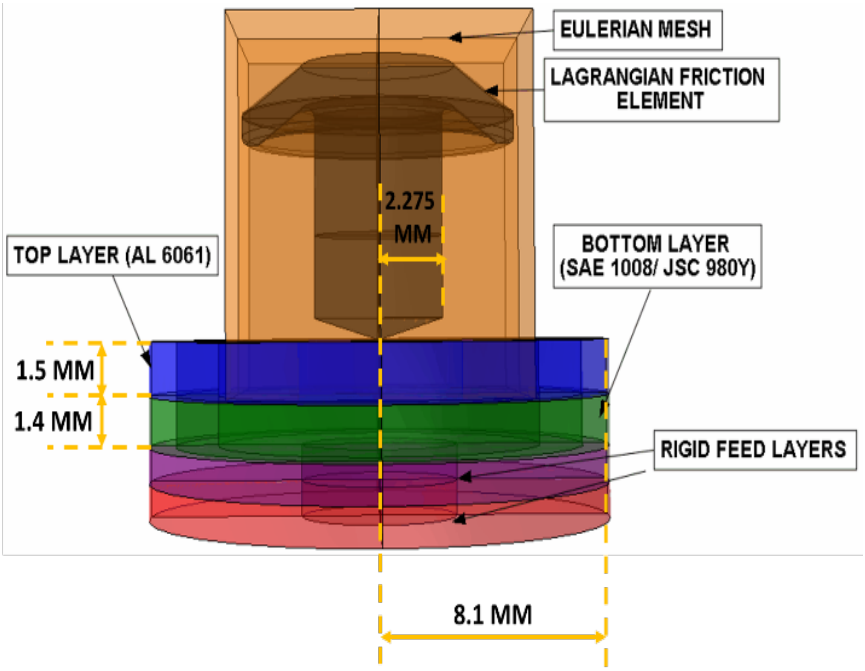

FIGURE 9 ASSEMBLY WITH DIMENSIONS OF DIFFERENT PARTS

3.1.1. ABAQUS/Explicit Solver:

In the current research work, an explicit central-difference time integration rule has been used in the numerical model. As per ABAQUS documentation[93], it is relatively inexpensive and suitable for models consisting of large rotations and deformation. One of the major disadvantage of the central-difference operator is that it is conditionally stable meaning that the stability limit is subjected to vary significantly resulting in very small stable time increments which can, in some cases, make the approach computationally expensive or infeasible. According to the ABAQUS documentation, an approximate rule for determining the stability is

defined as the smallest transit time required by a dilatational wave to travel across an element in the mesh, which is mathematically expressed as

$$\Delta t = {}^{L_{min}}/_{C_d}$$

where L_{min} is the smallest element dimension in the mesh and C_d is the dilatational wave speed in terms of Lame's constants.

The specification of element mesh size directly influences the stable time increment and thereby the computational time. The mesh size should be optimal such that the computational time can be minimized while maintaining desirable level of accuracy. The time incrementation in ABAQUS/Explicit can be specified in multiple ways i.e. either it can be completely automated which allows the solver to regulate the time increment depending on the severity of deformation of elements or a fixed time incrementation can be used which will remain constant throughout the process irrespective of the amount of deformation of elements. The fully automated time incrementation approach gives flexibility to the solver to deal with distortion issues by modifying the stable time increment whereas in the case of fixed time incrementation, if the dilatational wave speed is smaller than the specified time increment it would result in abrupt failure of the job. For the current research work, fully automated time incrementation option was utilized for the explicit solver as the amount of deformation an element undergoes increases significantly as the model progresses meaning that the stable time increment near the end of process can be significantly smaller than at the beginning of the process.

3.1.2. Material Behavior:

There are a number of material constitutive models available in the published literature for determining the materials' response to external loads but due to ease of availability of data for a wide variety of materials, Johnson-Cook constitutive law[94] was used to model the elastic-plastic response of different parts. The JC plasticity model is based on phenomenological observations and it multiplicatively combines the effect of strain, strain rate, and temperature on the flow stress of the material according to Eqn-1.

$$\sigma_y = \{A + B[\varepsilon^{-pl}]^n\}\{1 + C*\ln\frac{\dot{\varepsilon}^{-pl}}{\dot{\varepsilon}_0}\}\{1-[\frac{T-T_{ref}}{T_{melt}-T_{ref}}]^m\} \quad (1)$$

where, σ_y is the yield/flow stress, ε^{-pl} is the effective plastic strain, $\dot{\varepsilon}^{-pl}$ is the effective plastic strain rate, $\dot{\varepsilon}_0$ is the reference strain rate, T_{melt} is the melting temperature of material, T_{ref} is the reference temperature, and A, B, C, n, m are material constants. The constants of different materials used in this study are shown in TABLES 3 to 6.

TABLE 3 JOHNSON-COOK MODEL CONSTANTS FOR AL 6061 ALLOY[95]

A (MPa)	B (MPa)	C	n	m	$\dot{\varepsilon}_0$	T_m (K)
275	86	0.05	0.39	1	1	855

TABLE 4 JOHNSON-COOK MODEL CONSTANTS FOR SAE 1008 ALLOY[96]

A (MPa)	B (MPa)	C	n	m	$\dot{\varepsilon}_0$	T_m(K)
285	334	0.076	0.643	1	0.001	1808

TABLE 5 JOHNSON-COOK MODEL CONSTANTS FOR JSC 980 ALLOY[97]

A (MPa)	B (MPa)	C	n	m	$\dot{\varepsilon}_0$	T_m(K)
980	2000	0.0026	0.83	1.4	1	1643

TABLE 6 JOHNSON-COOK MODEL CONSTANTS FOR AISI 4340 ALLOY[98]

A (MPa)	B (MPa)	C	n	m	$\dot{\varepsilon}_0$	T_m(K)
1430	2545	0.014	0.7	1.03	1	1793

To ensure that friction element completely drills through the top aluminum layer without facing any distortion issues, excessively distorted elements were removed from the simulation domain by making use of element deletion criteria available in ABAQUS. The Johnson-Cook failure criterion[40], wherein the strain at failure $'\varepsilon_f'$ is calculated as per Eqn-2 , was used to delete the elements which satisfied the prescribed condition. The element is deleted when the value of damage variable (D = $\varepsilon^{-pl}/_{\varepsilon_f}$) reaches 1 in case of linear damage evolution and 0.99 in case of exponential damage evolution. The parameters of JC failure criteria for the top layer are described in TABLE 7. The values of constants for JC plasticity and failure models are widely varying in the published literature. As such, values from different research papers for the same material were analyzed for their effect on the FEM outputs and chosen accordingly.

$$\varepsilon_f = \left[d_1 + d_2 exp\left(d_3 \frac{\sigma_p}{\sigma_e}\right)\right]\left[1 + d_4 ln\left(\frac{\dot{\varepsilon}^p}{\dot{\varepsilon}_0}\right)\right] \times \left[1 + d_5\left(\frac{T - T_{room}}{T_{melt} - T_{room}}\right)\right] \quad (2)$$

where, ε_f is the failure strain, $\dot{\varepsilon}^p$ is the plastic strain rate, $\dot{\varepsilon}_0$ is the reference strain rate, σ_p is the mean stress, σ_e is the Mises stress, $\frac{\sigma_p}{\sigma_e}$ is the stress triaxiality, and d_1 to d_5 are material failure parameters, respectively.

TABLE 7 JOHNSON-COOK FAILURE MODEL CONSTANTS FOR AL-6061[98]

d_1	d_2	d_3	d_4	d_5	T_m(K)	T_{room}(K)
0.071	1.248	1.142	0.147	0	855	298

3.1.3. Frictional Behavior:

The frictional behavior between the workpiece layers and the friction element is realized using the Coulomb's modified friction law which takes the shear stress limit into consideration to decide whether the interacting surfaces will stick or slip against each other. The value of shear stress limit is generally calculated as '$\sigma/\sqrt{3}$' where 'σ' is the initial yield strength of the material. It has to be noted that this value of shear stress limit remains unchanged for the entire process and is based only on the initial yield strength of the concerned material. The stick/slip condition is calculated as per equations-3 and 4.

$$\tau < \frac{\sigma}{\sqrt{3}} \ (sticking\ condition) \tag{3}$$

$$\tau \geq \frac{\sigma}{\sqrt{3}} \ (sliding\ condition) \tag{4}$$

whereas the frictional stress in these regions is calculated as

$$\tau = \mu N \ (sticking\ region) \tag{5}$$

$$\tau = \frac{\sigma}{\sqrt{3}} (slipping\ region) \tag{6}$$

where τ is the frictional stress, N is the normal stress, and μ is the coefficient of friction, respectively.

The value used for friction coefficient varies widely in the published literature, from 0.2 to 0.6 and higher, depending on the type of process being analyzed, materials being

used, and the required heat generation characteristics[60,80,99]. The relationship between variation of friction coefficient with temperature, contact pressure, etc. is not yet fully developed and experimentally verified which makes the employment of a variable friction coefficient less reliable. The value of friction coefficient directly affects the heat generation and the temperature reached in different parts. In the current study, different values of friction coefficient ranging from 0.1 to 1 were analyzed for their effect on the FEM outputs and the resulting temperature was compared against the experimental observations after which a constant value of 0.4 was adopted for all models. The shear stress limit used in the current study is 159 MPa and as mentioned earlier, it remains constant throughout the numerical simulation. It has been assumed that 100% of the friction dissipated energy is converted into heat and the distribution of this friction heat between the workpiece layers and the friction element is calculated based on their density, specific heat, and thermal conductivity, as reported in [87]:

$$H_{w/p} = \frac{\sqrt{\rho c k}_{w/p}}{\sqrt{\rho c k}_{tool} + \sqrt{\rho c k}_{w/p}} \quad (7)$$

where $H_{w/p}$ is the heat transferred to workpiece, ρ is the density, c is the specific heat, and k is the thermal conductivity.

Due to the presence of high amount of plastic deformation of different materials in the process, heat generation resulting from it is also considered as a heat source wherein the inelastic heat fraction is specified the default value of 0.9.

3.1.4. Contact Definition:

The ‘general contact’ algorithm which can efficiently handle interactions between multiple surfaces of both Eulerian & Lagrangian parts is used for defining the contact between different parts. Between the two workpiece layers, their tangential interaction is governed by Coulomb’s friction law with a constant friction coefficient of 0.4 while the interactions in the normal direction is defined using a ‘hard’ contact which allows for transmission of pressure across the surfaces as well as separation of the surfaces, thereby depicting experiment like conditions. Sticking behavior was defined between the two rigid layers (used for providing the feed) and the bottom steel layer. As there is no interaction between the top aluminum layer and the two rigid layers, no contact definition is required and hence, none is defined for this pair. Sticking behavior was also defined between the two layers of workpiece but only near the outer edges (red colored region in Figures 4 & 5) with the aim of replicating the ‘downholder’ i.e. ensuring that no gap occurs between them. Specification of sticking behavior over a large surface area between the two layers of workpiece is avoided as it would adversely affect the element deletion and lead to element distortion.

3.1.5. Boundary Conditions & Loads:

It is computationally difficult to provide rotational and translational velocities to the Eulerian friction element which would require a mesh of substantially large domain to contain the rotating material leading to computational time issues. As such two additional

layers which are defined to be rigid throughout the process and having the dimensions identical to the bottom steel layer are used to provide the rotation and translation to the workpiece in the FEM. These two rigid layers are placed at the bottom of the configuration i.e. below the steel layer. By making use of 'sticking' contact condition between the layers as discussed earlier, motion is transmitted from one part to another against the stationary friction element. In the experimental results, it was observed that the upper portion of the friction element remains relatively deformation-free. Based on this observation, the upper portion of the friction element was fully constrained with respect to all mechanical degrees of freedom. This boundary condition is aimed at achieving two objectives: firstly, to prevent unexpected displacement of friction element against the moving workpiece and secondly, to reduce the computational time by removing nodes from calculations that do not experience deformation or are of less importance. The layers of the workpiece are not constrained by any type of boundary condition and are free to move in any direction. In the experiments, a downholder has been utilized to prevent any gap formation between the aluminum and steel layers, but in the current FEM setup the workpiece layers are being fed against the stationary friction element. Replicating the downholder using a boundary condition or a load or a rigid part would effectively act against the specified motion of workpiece layers. As stated in 'contact definition', sticking behavior was utilized instead of using a boundary condition to prevent any gap formation between the layers. It has to be noted that the region over which sticking contact is defined is limited and it does not cover the interaction region to avoid any computational difficulty. The rigid layers are constrained to rotate and translate only in the z–direction using the velocity/angular

velocity boundary condition. Convection and radiation heat losses from the surface of different parts are not considered in this study since the total processing time is very short. An initial reference temperature of 298 K is assigned to all the parts. The Eulerian entity for the friction element is created using the volume fraction tool which requires a Lagrangian object for reference purpose. The Lagrangian friction element is placed inside the Eulerian mesh domain and the volume fraction tool calculates the amount of space occupied by the reference object for each Eulerian mesh element and creates the geometry based on it. The occupancy magnitude varies from 0 to 1 wherein 0 denotes the Eulerian mesh cell is completely empty and 1 indicates that the cell is fully occupied by reference object.

The process parameters used in the FEM for validation against the experimental deformation and temperature evolution are described in TABLES 7 and 8. Two separate sets of process parameters were utilized because the thermal sensors used for temperature measurements were developed at a later stage by Dr. Hongseok Choi[100] & his research group at Clemson University. Readers interested in their work can find more about their work in [100].

TABLE 8 SET-1: PROCESS PARAMETERS FOR PHYSICAL DEFORMATION VALIDATION

Step	Feed velocity (mm/s)	Rotational speed (RPM)	Time (s)
penetration	7.74	5000	0.168
cleaning	2.16	5500	0.371
welding	18	6000	0.061
compression	10	0	0.243

TABLE 9 SET-2: PROCESS PARAMETERS FOR TEMPERATURE EVOLUTION VALIDATION

Step	Feed velocity (mm/s)	Rotational speed (RPM)	Time (s)
penetration	7.35	5000	0.177
cleaning	1	4000	0.798
welding	9.82	4000	0.112
compression	2	0	0.3

3.1.6. Mesh:

In order to simultaneously evaluate the thermal and mechanical history of the parts, they are meshed with 8-node thermally coupled brick, trilinear displacement and temperature based elements ‘C3D8RT’ and ‘EC3D8RT’ for Lagrangian and Eulerian objects respectively (except the two rigid layers). To obtain an accurate representation of the friction element and its deformation, it is necessary that the Eulerian mesh is finer when compared to other parts. As such, the mesh density for the Eulerian mesh is highest when compared against the Lagrangian meshes. With respect to mesh density for Lagrangian objects, it is required that top aluminum layer has relatively finer mesh than the other layers to facilitate efficient removal of elements without losing excessive amount of material from it. The mesh densities for the rigid layers, providing feed, is the lowest with the about 500 elements in each of them. To address the issue of hourglassing in different parts, a combination of ‘stiffness’ and ‘viscous’ hourglass controls were used. The bottom steel layer also experiences considerable amount of deformation which can possibly cause element distortion, but the magnitude of deformation in it does not warrant the use of element deletion. Therefore, to aid in maintaining the shape of elements of bottom steel layer, distortion control for its mesh elements was specified. The mesh density was varied in different regions within a part because the interaction and deformation region was concentrated in an area slightly larger than friction element diameter. For workpiece layers as we move outwards from the center, the mesh density keeps decreasing while for the friction element as we move upwards from the bottom, the mesh density decreases significantly with the bottom portion having most number of elements. Choosing the

appropriate mesh density for the parts involved in interaction is highly critical to achieve an accurate output each time. The mesh densities of the parts were varied from very high to very low values and the subsequent effect on the FEM results were analyzed. It was observed that using too fine of a mesh is unfeasible because of very long computational time running into months whereas for a coarse mesh the FEM couldn't run the specified process time due to distortion issues. After analyzing the results from different FEMs and taking into account the computation time, mesh density for different parts was specified as per TABLE 10. The meshed parts are shown in FIGURES 10-12.

TABLE 10 MESH DENSITY OF DIFFERENT PARTS

Part	Number of elements
top layer	18,000
bottom layer	6,000
friction element	64,000

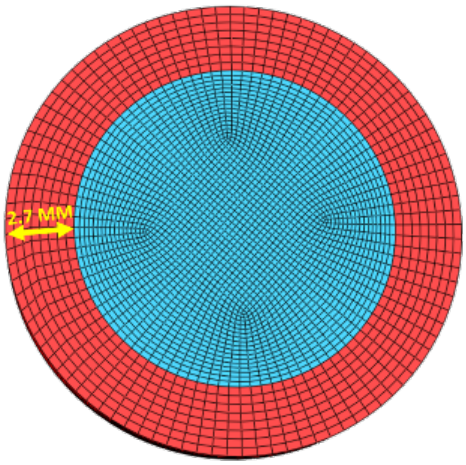

FIGURE 10 TOP LAYER

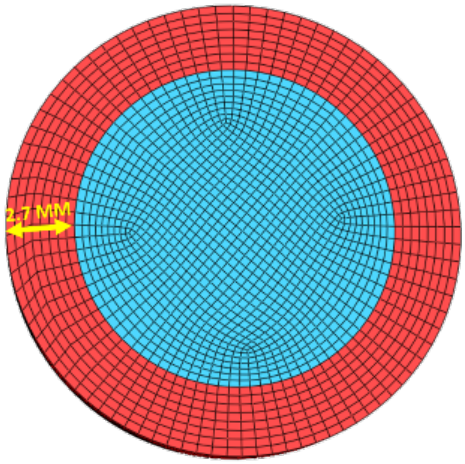

FIGURE 11 BOTTOM LAYER

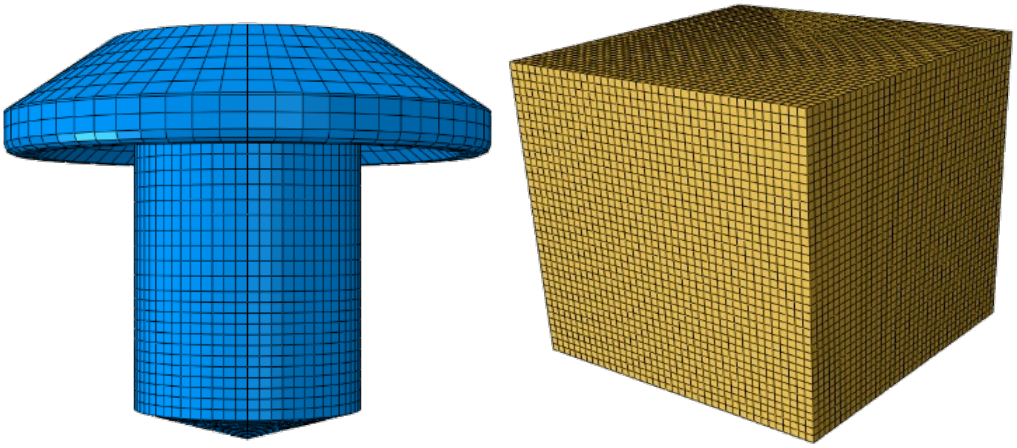

FIGURE 12 FRICTION ELEMENT MESH,

LAGRANGIAN ENTITY (LEFT) & EULERIAN ENTITY (RIGHT)

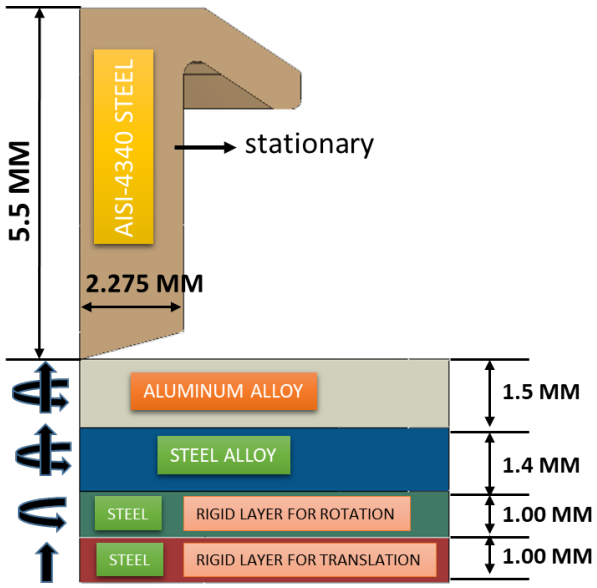

FIGURE 13 CROSS-SECTION OF FEM SET-UP WITH

DIMENSIONS OF DIFFERENT PARTS

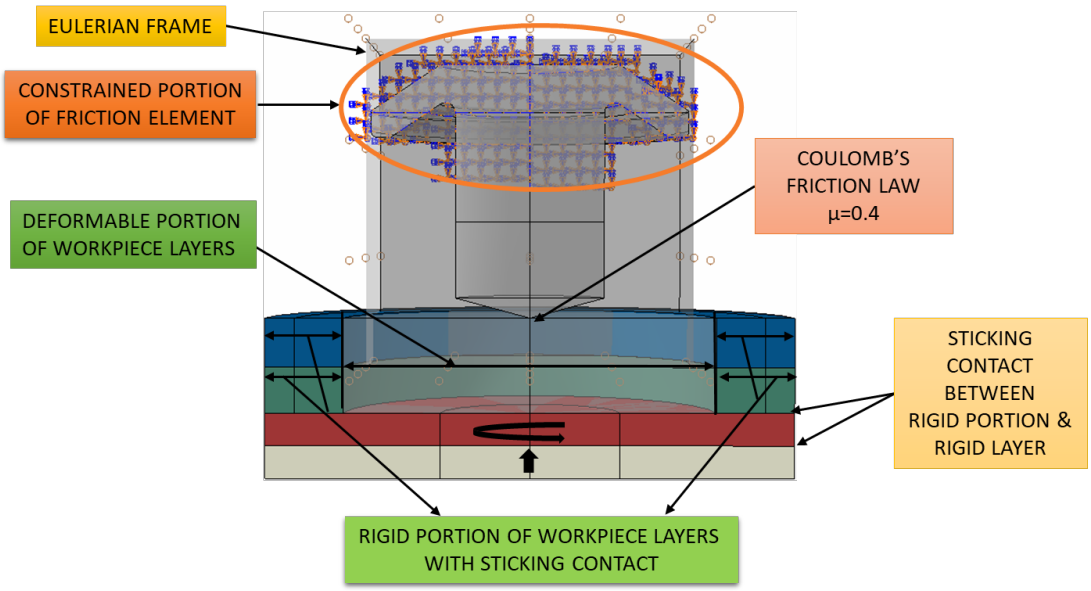

FIGURE 14 CROSS-SECTION OF FEM SET-UP REPRESENTING DIFFERENT

INTERACTIONS AND LOADS

3.1.7. Computational Time:

As mentioned earlier, the elements of the friction element as well as workpiece will undergo high amount of deformation which would result in very small time increments. For example, the stable time increment decreases from 2E-08 s to 1E-10 s or even lower values as the mesh deforms. With such low value of time increments, the total computational time for simulating the entire FEW process can run into months. Manually controlling the time increment is rather difficult for a non-linear transient process such as FEW which leaves the user with option of either artificially decreasing the simulation time or using the option of mass scaling provided by ABAQUS. Hammelmüller et al.[101] studied the feasibility of reducing computational time for an CEL model by using time scaling as well as mass scaling and stated that artificial reduction of the real process time is practical only when the strain rate effects are negligible thereby making this option unviable for a dynamic process involving materials with high strain rate dependency. In case of time scaling being used for a dynamic process such as FEW, it must be ensured that the overall effect of reducing the time is compensated by increasing other physical parameters involved in thermo-mechanical calculations in order to maintain the global balance of equations and obtain outcome similar to that of a non-scaled model. As per ABAQUS documentation, in cases of dynamic analyses the mass of certain elements, undergone or undergoing, extreme deformation can be artificially scaled using different available options to improve computational efficiency without effecting the accuracy of the results. However, there is one limitation with respect to using CEL approach i.e. the mass of Eulerian elements cannot be scaled by ABAQUS while the process is running,

which means that the mass has to be scaled explicitly in the pre-processor itself. The magnitude by which the mass should be scaled is entirely dependent on the user's discretion and there are no hard rules to decide upon a certain magnitude. Extreme care must be taken when deciding about the magnitude of either time scaling or mass scaling as unusually high amount can result in physically meaningless results.

In the current wok time scaling method, wherein the total process time is reduced by a pre-determined factor by artificially increasing the speed with which loads are applied, has been used. To make the simulation comparable to the experiment, all the physical equations involved in this model are rewritten into dimensionless scale, and the physical parameters are adjusted accordingly to guarantee that the calculation results are the same as the case with real scale. After running a number of simulations with different scaling factors and analyzing the results with respect to different physical parameters for their accuracy and also by checking the energy balance[101,102], a scaling factor of 10 was chosen for all the FEMs. After deciding on the scaling factor, another analysis was carried out to find the optimal number of cores that completed the entire simulation in minimal time repeatedly for different sets. The number of cores were varied from as low as 16 to the maximum available number of 256 for a given FEM setup. It was found that specifying the number of cores to be between 32 to 64 yielded better computation time when compared to using a quantity lower than 32 or more than 64. The lowest computation time was observed for the FEM submitted using 64 cores and therefore, for all the FEMs submitted we have used the same number of cores i.e. 64.

CHAPTER FOUR
RESULTS AND DISCUSSIONS

4.1. Material Deformation:

Before progressing towards the validation of the FEM results, a comparison between two CEL models is made which establishes the need for defining the friction element as a Eulerian entity instead of the conventional Lagrangian one. The two FEMs, one with Eulerian friction element and the other with Lagrangian friction element, have the same parameters defined as described in TABLE 7. The comparison is made with respect to their material deformation (refer FIGURE 15), which signifies the fact that the extreme amount of plastic straining present in FEW process is well captured by the Eulerian mesh without any issues.

(A)

(B)

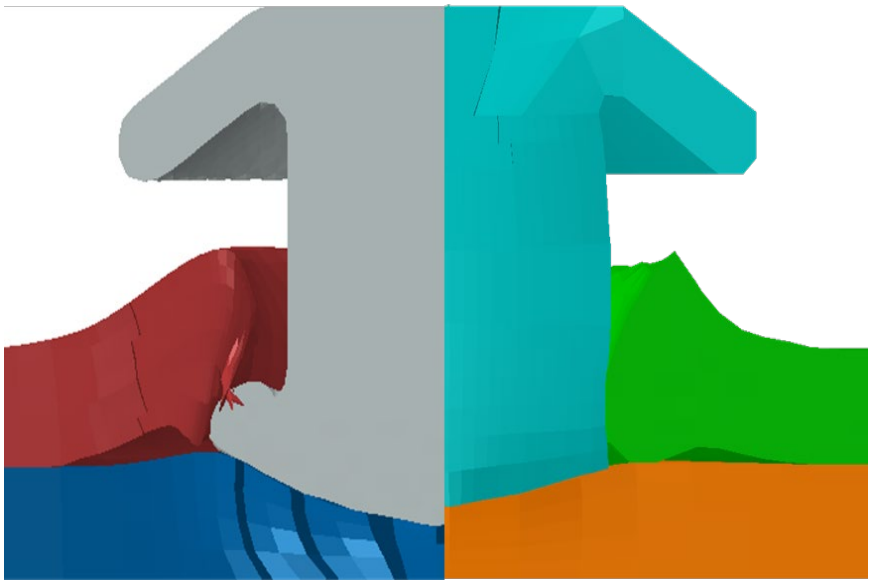

(C)

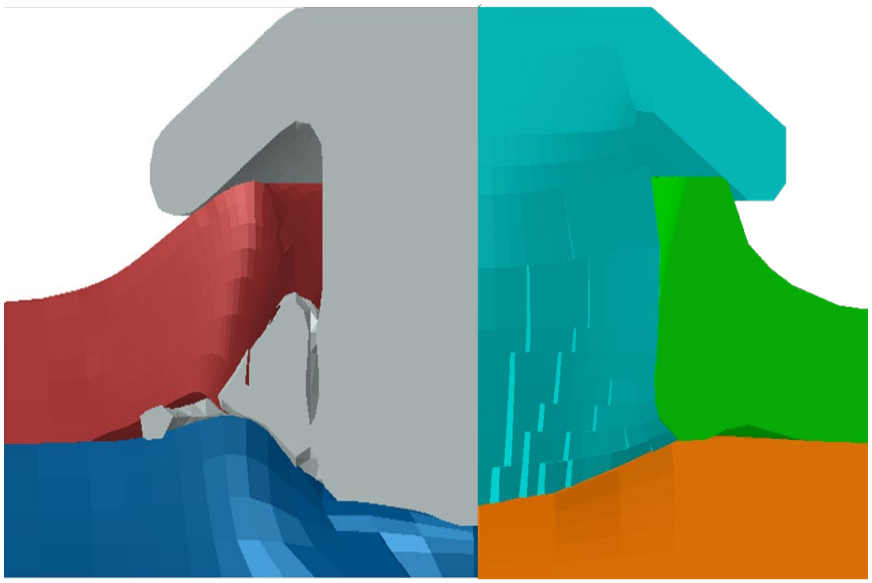

(D)

FIGURE 15 COMPARISON OF FEM RESULTS WITH EULERIAN FRICTION ELEMENT (LEFT) AND LAGRANGIAN FRICTION ELEMENT (RIGHT) AT END OF (A) PENETRATION (B) CLEANING (C) WELDING AND (D) COMPRESSION

As can be observed in above figures, the deformation of Lagrangian friction element is completely different from that of the experimental results as well as from that of Eulerian friction element. The Lagrangian friction element is unable to plastically deform under the applied endload and deform laterally thereby forming the necessary weld.

Friction element deformation is of critical importance for FEW, since it introduces the mechanical inter-lock weld for the process. It is essential to understand the material deformation process through the FEM analysis. Using the parameters from TABLE 7, an

FEM was submitted to verify the deformation achieved in the simulation against the experimental results obtained for the same set of parameters. A comparison of the material deformation achieved in the FEM (left column) against the experimental results (right column) measured using an optical microscope can be seen in FIGURE 16. It can be observed that during the penetration step, the shape of the friction element does not change significantly, which can be attributed to two factors. First, low friction heat generation and consequently lower temperatures are generated during the interaction of soft aluminum layer and hard steel element. Second, the higher thermal conductivity of aluminum layer than that of steel friction element results in more heat conduction into the former than latter. By the end of second step, Cleaning, the element has already drilled through the aluminum layer and subsequently interacts with the bottom steel layer. Due to the strong friction interaction between the steel element and the steel layer, high temperatures are generated which initiates plastic deformation at the bottom of the element as well as heating of the steel layer. In the next step, Welding, under the application of increased rotational speed and endload, the friction interaction between the element and steel layer is amplified which results in heating of friction element & steel layer to a much higher temperature and consequently significant deformation of bottom portion of the element (FIGURE 16-C). The lateral deformation of friction element will displace the surrounding aluminum material which would ultimately help fill the gap under the friction element head. Due to the presence of high temperature and plasticized materials, a weld begins to form near the interaction zone during this step. In Compression step, there is no element rotation, but a strong load force is applied to push the element down against the steel layer which induces

further deformation of the element. The aluminum material displaced towards the element shoulder head mechanically interlocks with the element. For each step, the dimensions of the deformed part obtained in the FEM agree well with that of experimental observations.

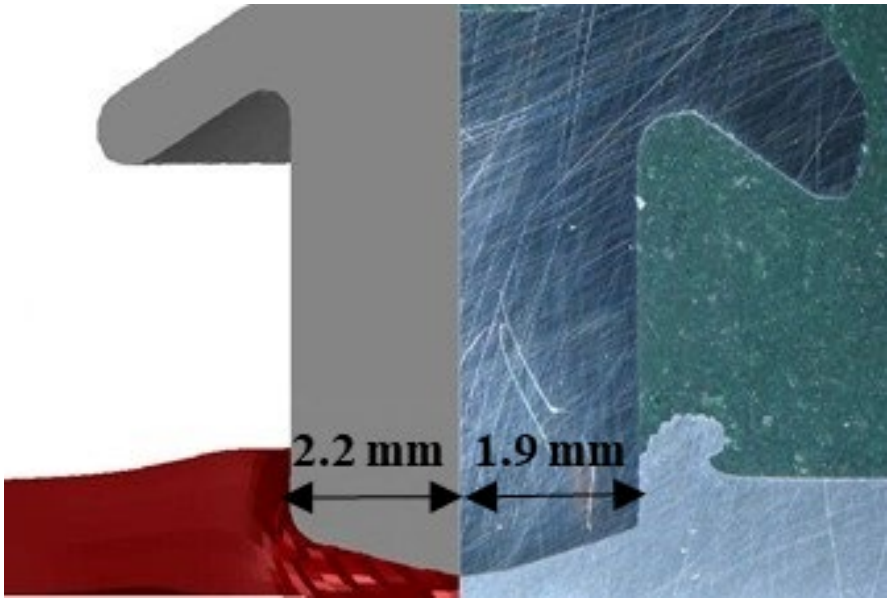

(A)

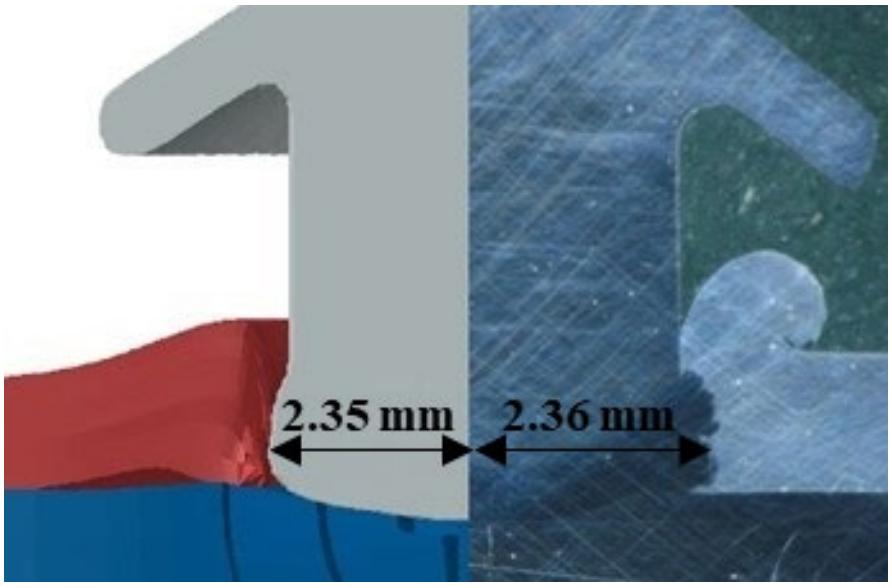

(B)

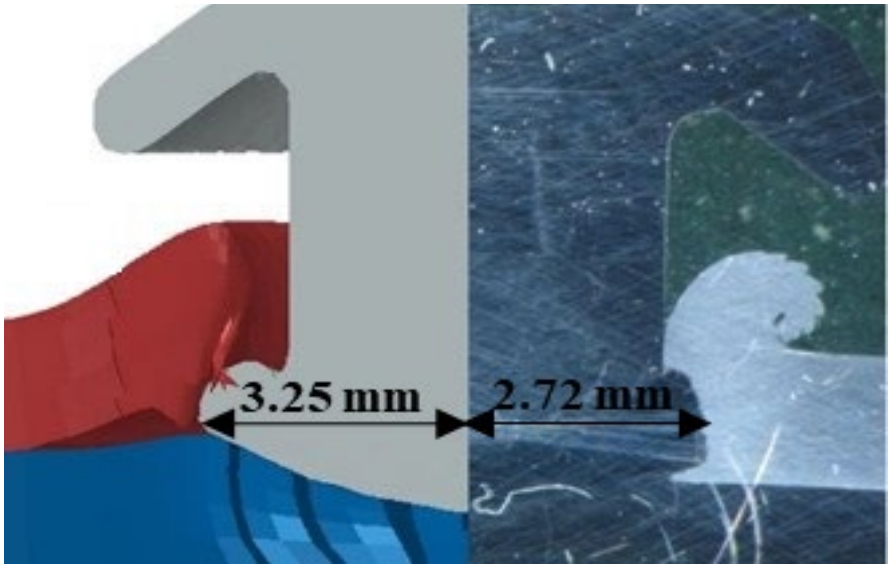

(C)

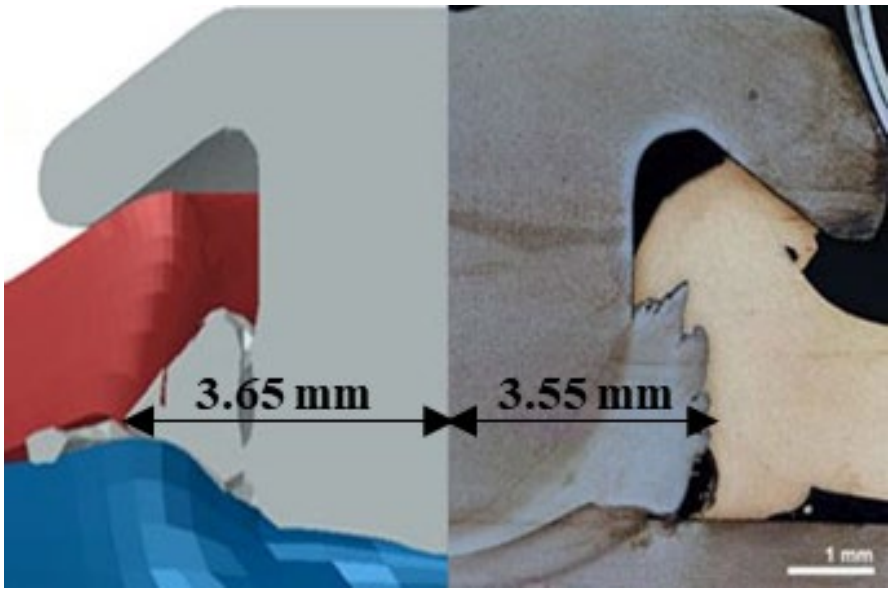

(D)

FIGURE 16 CROSS-SECTION OF ASSEMBLY AT THE ENDS OF (A) PENETRATION (B) CLEANING (C) WELDING AND (D) COMPRESSION. THE LEFT SIDE IS THE SIMULATION RESULTS, AND THE RIGHT SIDE REPRESENTS MEASURED IMAGES BY AN OPTICAL MICROSCOPE

4.2. Temperature Evolution:

To further validate the developed FEM, another model using the parameters from TABLE 8 was submitted for the purpose of comparison of temperature evolution at different points against the measurements obtained experimentally for same set of parameters as in the FEM. As mentioned earlier in finite element modeling section, the experimental measurements for temperature at different locations were provided by the research group of Dr. Hongseok Choi[103]**.** Due to the highly transient nature of the FEW

process, thermal sensors were placed at different locations at the interface of the two layers of workpiece to avoid any damage to them and obtaining meaningful readings. The placement of thermal sensors is shown in FIGURES 18 to 20. Three sensors starting at 2.275 mm (equal to radius of friction element), 4.9 mm, and 5.775 mm away from the element center were placed to measure the transient temperature evolution and the extent to which heat is dissipated within the workpiece layers. In FIGURE 18, the comparison between the FEM results and the experimental measurements can be seen. Since the thermal couple is on the interface between two layers, its temperature should be affected by both layers. Therefore, the temperature of the bottom surface of the first (aluminum) layer and the top surface of the second (steel) layer at the same location are both calculated, and their average is used to be compared with the sensor measurement. It can be seen that the FEM results at 2.275 mm and 4.9 mm locations agree well with thermal sensor measurement while at the location of 5.775 mm the simulation result reaches a higher magnitude earlier than the experimental result. Due to the absence of heat loss in the form of convection or radiation, the simulation results tend to be higher than the experimental result but the difference between the two isn't significant proving that the FEM model can predict the material deformation and temperature evolution with considerable accuracy. At 2.275 mm, temperature remains at about room temperature for about 0.05 s since the heat generation occurs in the interaction zone at a distance far away from the sensors' location. As sufficient heat is generated due to friction interaction between the friction element & the aluminum layer, the temperature rises rapidly by more than 250 K by the end of Penetration. During the Cleaning step, the temperature further increases by 250 K to reach

first peak value of 500 K as the element drills its way through the aluminum layer and at 0.45 s the temperature drops by 75 K due to absence of material, for friction interaction, from the path of element. As the friction element makes contact with the bottom steel layer under the presence of uniform rotational speed and endload, the temperature reaches a steady state at about 414 K and remains around the same magnitude until 0.83 s. Under the effect of friction heat generation between steel element and steel layer, the temperature increases by about 80 K by the end of Cleaning. In the Welding step, as a result of sufficient time for the friction interaction between the steel element-steel layer and heating in the previous step, the temperature experiences a sharp increase of more than 530 K i.e. it increases from 495 K to about 1040 K. As the rotational feed is cutoff to the element in the Compression step and high endload is applied, the temperature drops by about 200 K within 0.02 s and then tends to decrease rapidly to a steady value of about 700 K while dissipating heat within the workpiece layers as well as to the friction element. Considering the temperature evolution at locations of 4.9 mm and 5.775 mm, temperature remains at initial value of 298 K until 0.05 s and then steady increase by a magnitude of more than 100 K is observed until 0.48 s. The temperature then remains steady at a value of 414 K and 410 K till the end of Welding step, at 4.9 mm and 5.775 mm respectively. As there is significant displacement and deformation of material in the last step, the temperature away from the interaction region experiences a rapid increase in its magnitude to reach a peak value of 460 K and 450 K at 4.9 mm and 5.775 mm locations respectively. For the experimental measurements, meaningful increase in the temperature occurs at a later stage when compared with that of FEM result and as such the initial excessive data generated using

thermal sensor was deleted which resulted in shorter experimental process time for comparison purpose.

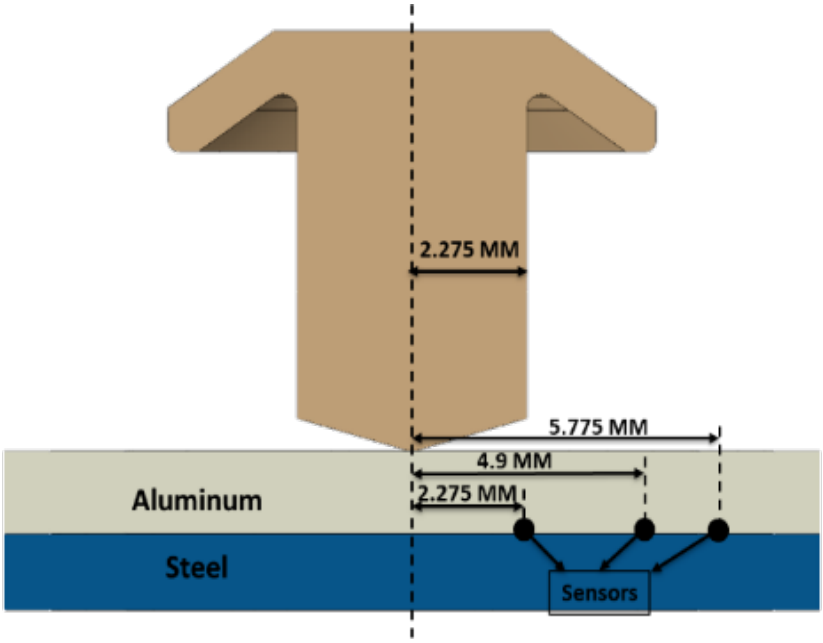

FIGURE 17 THERMAL COUPLE LOCATIONS FOR TEMPERATURE EVOLUTION MEASUREMENT

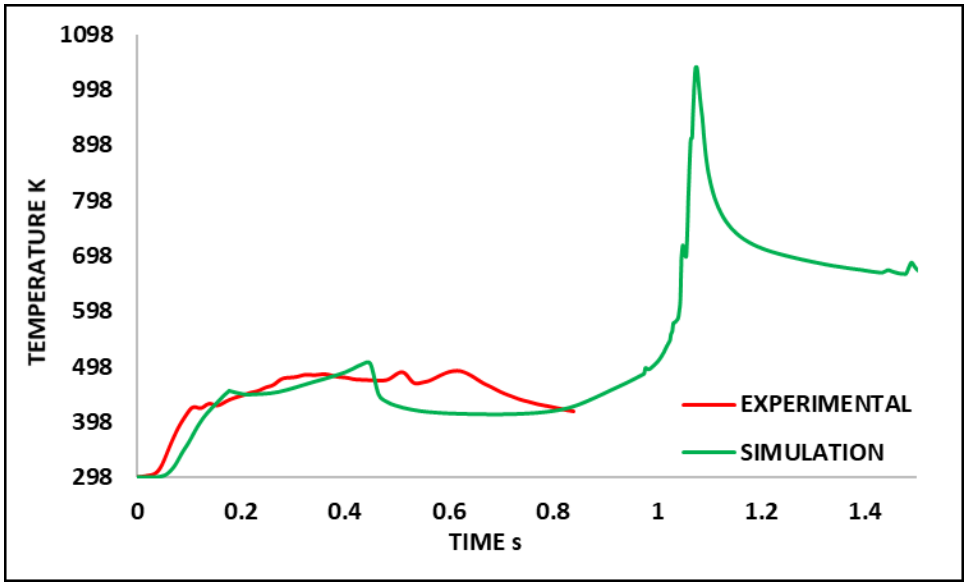

FIGURE 18 FEM VS. THERMAL SENSOR MEASUREMENT

AT A DISTANCE OF 2.275 MM AWAY FROM CENTER

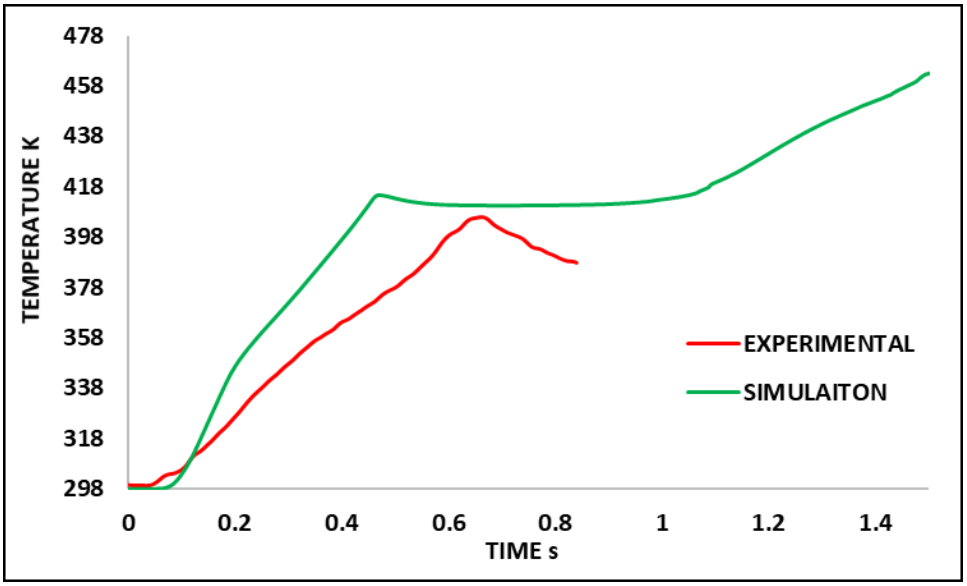

FIGURE 19 FEM VS. THERMAL SENSOR MEASUREMENT

AT A DISTANCE OF 4.9 MM AWAY FROM CENTER

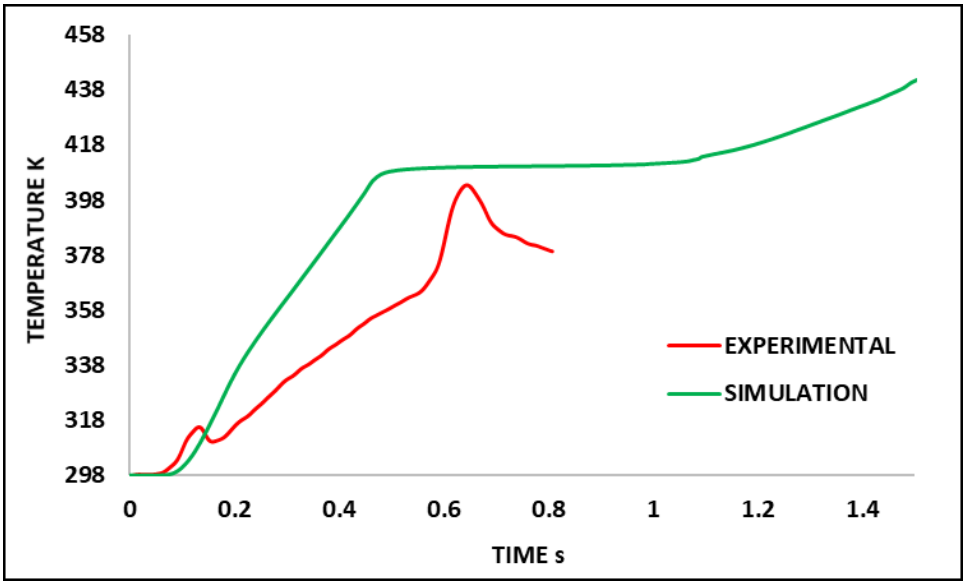

FIGURE 20 FEM VS. THERMAL SENSOR MEASUREMENT

AT A DISTANCE OF 5.7 MM AWAY FROM CENTER

The temperature distribution of friction element and workpiece at the end of different steps is shown in FIGURES 21-24. The detailed temperature distributions of the aluminum layer, steel layer, and the friction element are shown in FIGURE 25-27. By the end of Penetration, the highest temperature in the first layer is around 700 K to 750 K in the region where it interacts with the friction element. It is much lower than its melting point of 855 K and there should be no melting of the aluminum layer. The temperature of the second layer remains around the room temperature during this stage due to absence of thermal conductance between the two layers. In the meantime, the temperature of the friction element bottom portion rises to more than 900 K with a highest temperature of 1000 K observed at the outer region of its bottom surface where linear velocity will be the

highest. As the element continues drilling through the aluminum layer in the Cleaning step, the temperature of both the parts keeps increasing until there is element deletion (material failure) from the heated and deformed aluminum layer. In the same step as the aluminum layer is removed from the path of the steel element, it makes contact and interacts with the steel layer which is still at room temperature. Due to the strong friction interaction between steel element and steel layer, the temperature in steel layer increases to more than 1250 K whereas the temperature in the element reaches a peak value of 1300 K by the end of Cleaning. Temperatures as high as 425 K to 450 K are observed in the friction element shoulder head which is due to factors such as long step time and sufficient friction interaction, firstly with aluminum layer and then with steel layer. With respect to steel layer, the friction interaction period by the end of Cleaning is relatively small and the heat generation is concentrated near the upper surface and is spread in a narrow region slightly larger than the diameter of the element. It is important to note that the shape of the friction element even after reaching a peak value of about 1300 K, by the end of Cleaning, is well maintained. Under the influence of heightened friction based heat generation between steel element and steel layer, peak temperatures of more than 1700 K and 1750 K are observed in the element and the steel layer respectively, both of temperature values are near their respective melting points. By the end of Welding, the friction element is heated sufficiently so as to initiate the localized plastic deformation at the bottom region and a weld begins to form at the interface of element-layer. The extent of region in which heat is conducted within the steel layer does not vary significantly between the Cleaning and Welding steps as the heat generation is focused near the top surface where element makes contact. In

Compression, as the element stops rotating, the heated steel element-steel layer bond together under the increased endload and the element undergoes significant deformation while simultaneously displacing the aluminum layer under its shoulder head, thus forming an interlock between the two layers and itself. The displaced aluminum layer also experiences an increase in temperature due to heat dissipation from the two steel parts. By the end of Compression, the temperature in steel layer near the interaction region drops to 700 K whereas for the element an increase in temperature is observed throughout its length and diameter which results in a temperature of about 500 K to 530 K in the shoulder head.

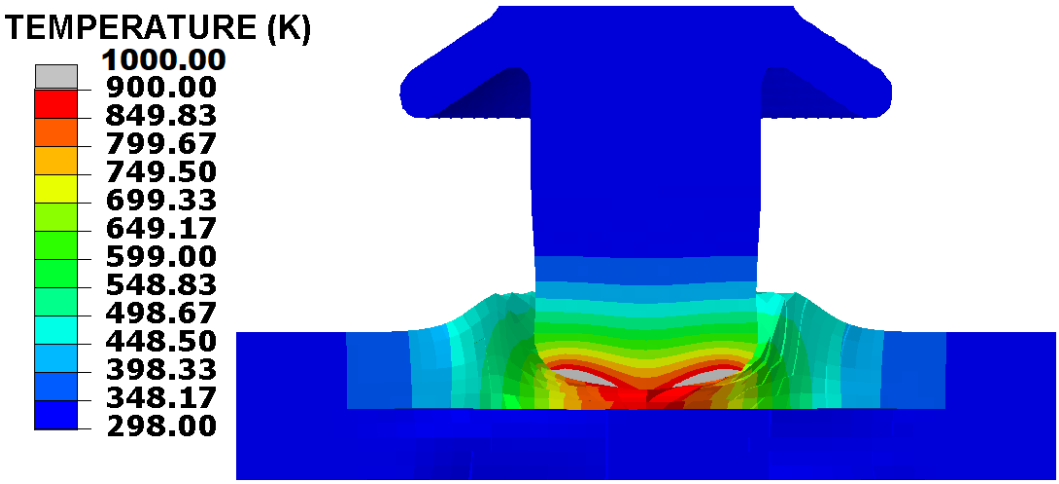

FIGURE 21 TEMPERATURE DISTRIBUTION & DEFORMATION

AT END OF PENETRATION

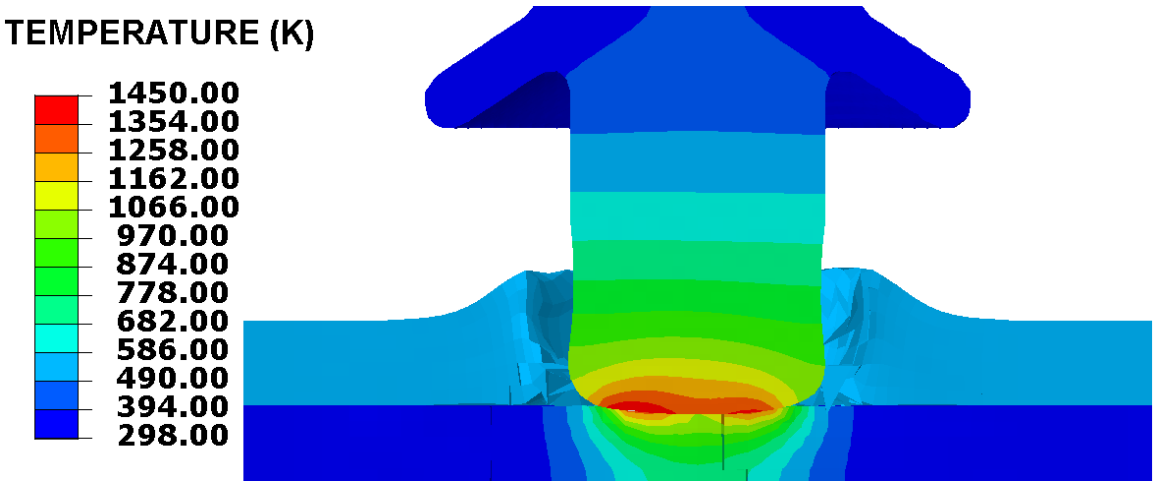

FIGURE 22 TEMPERATURE DISTRIBUTION & DEFORMATION

AT END OF CLEANING

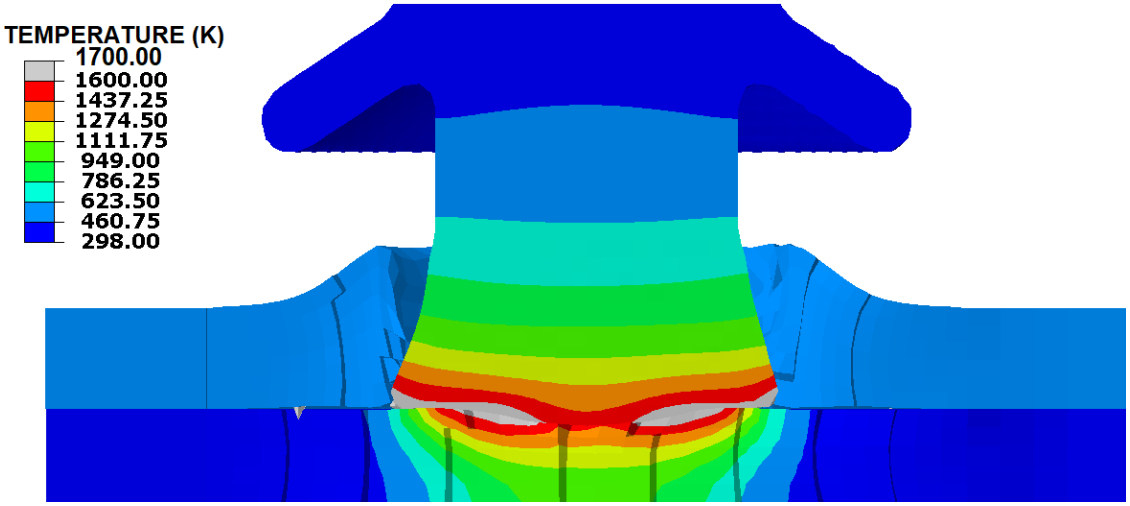

FIGURE 23 TEMPERATURE DISTRIBUTION & DEFORMATION

AT END OF WELDING

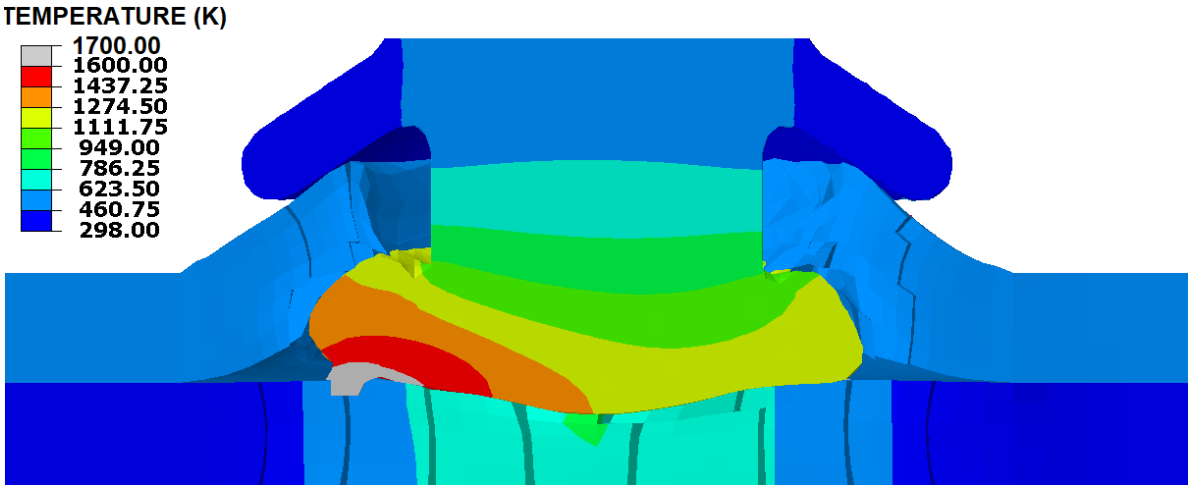

FIGURE 24 TEMPERATURE DISTRIBUTION & DEFORMATION

AT END OF COMPRESSION

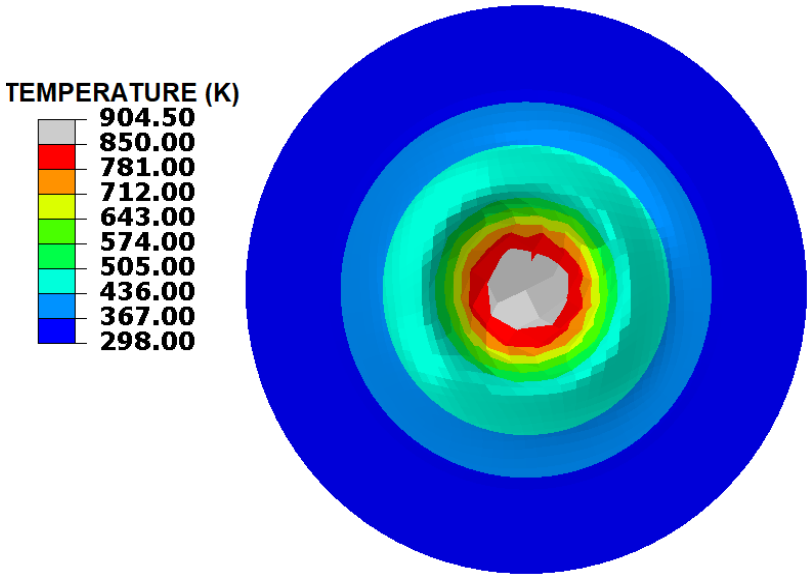

(A)

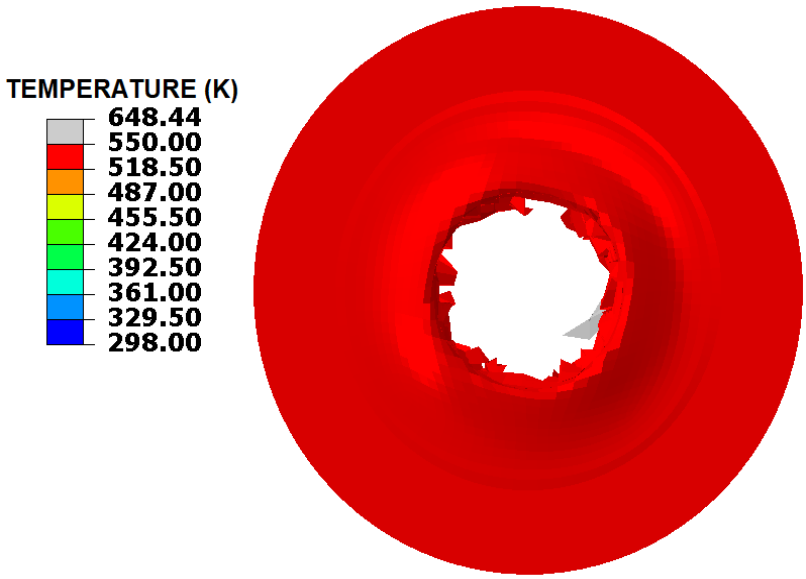
TEMPERATURE (K)
648.44
550.00
518.50
487.00
455.50
424.00
392.50
361.00
329.50
298.00

(B)

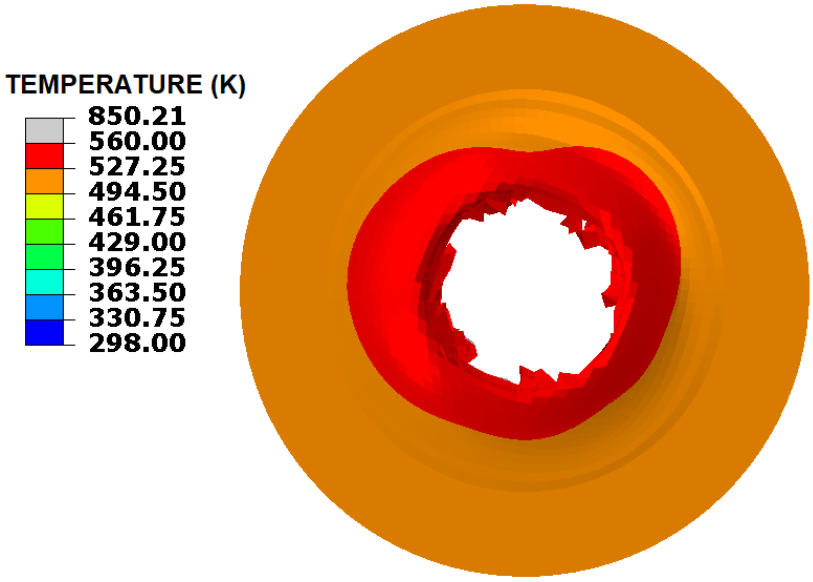
TEMPERATURE (K)
850.21
560.00
527.25
494.50
461.75
429.00
396.25
363.50
330.75
298.00

(C)

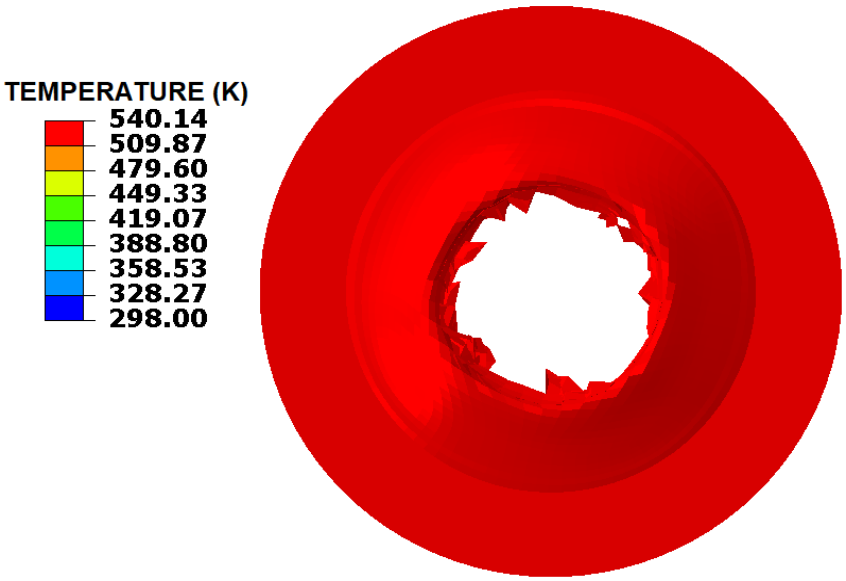

(D)

FIGURE 25 TOP VIEW OF TOP ALUIMINUM LAER, TEMPERATURE DISTRIBUTION AT END OF (A) PENETRATION (B) CLEANING (C) WELDING AND (D) COMPRESSION

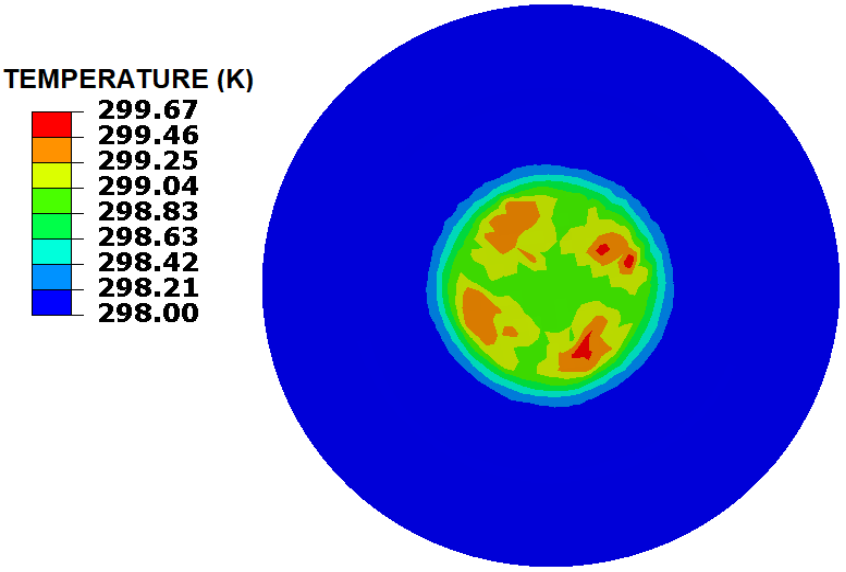

(A)

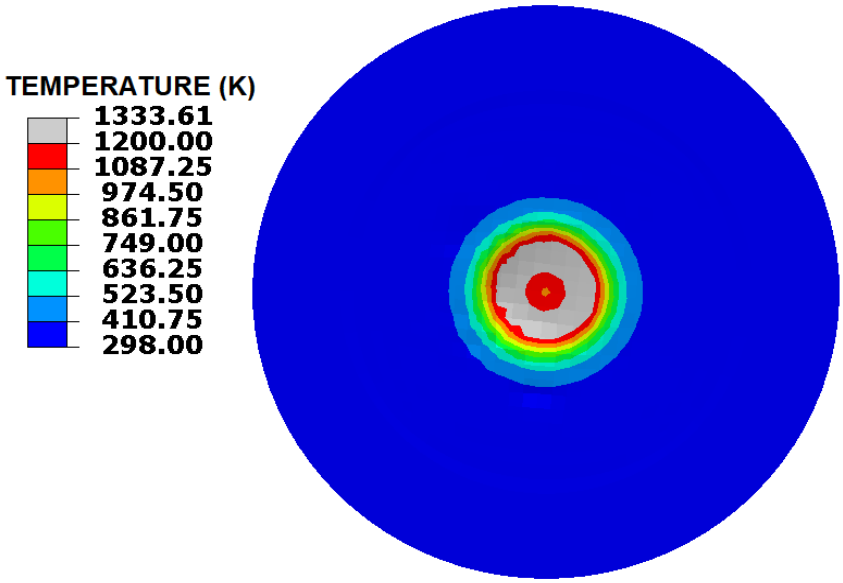
TEMPERATURE (K)
1333.61
1200.00
1087.25
974.50
861.75
749.00
636.25
523.50
410.75
298.00

(B)

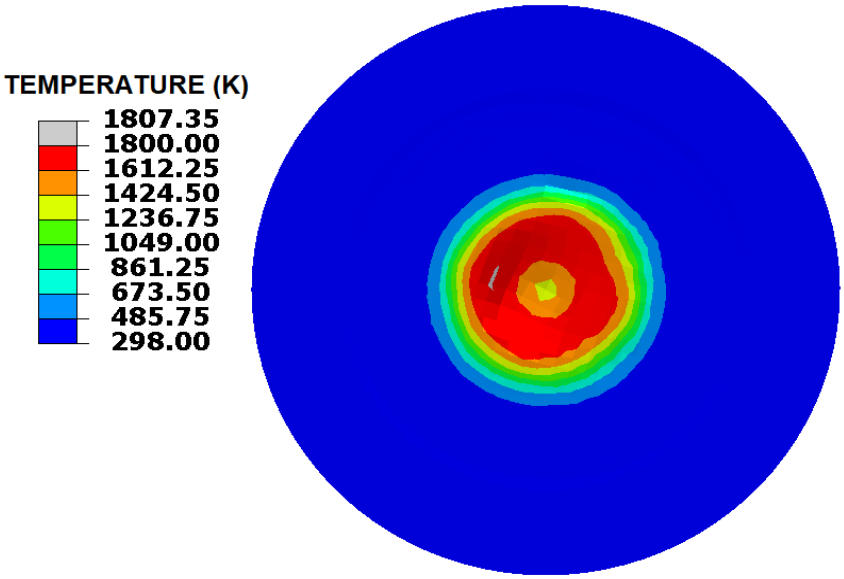
TEMPERATURE (K)
1807.35
1800.00
1612.25
1424.50
1236.75
1049.00
861.25
673.50
485.75
298.00

(C)

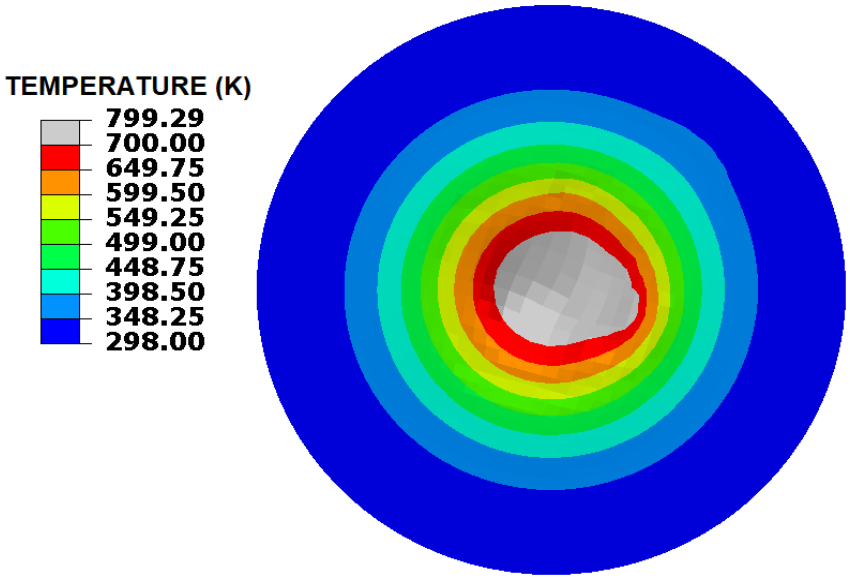

(D)

FIGURE 26 TOP VIEW OF BOTTOM STEEL LAER, TEMPERATURE DISTRIBUTION AT END OF (A) PENETRATION (B) CLEANING (C) WELDING AND (D) COMPRESSION

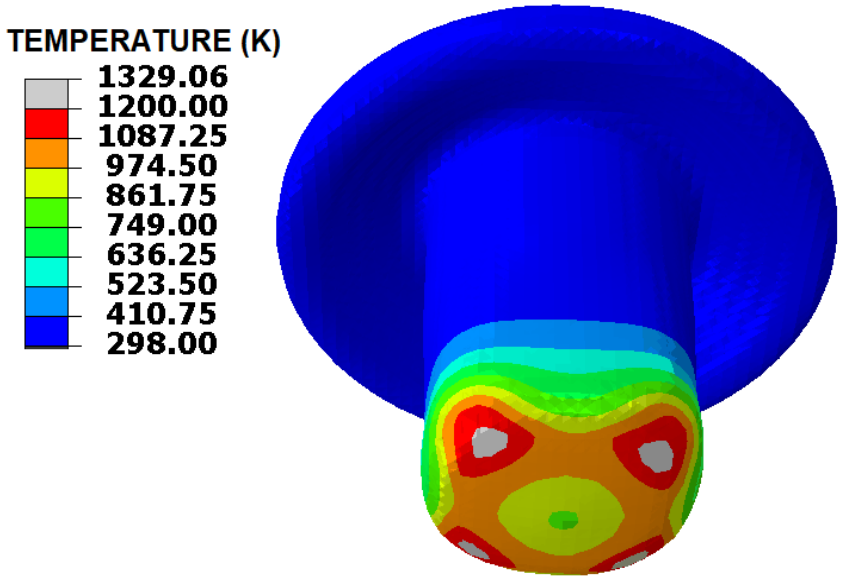

(A)

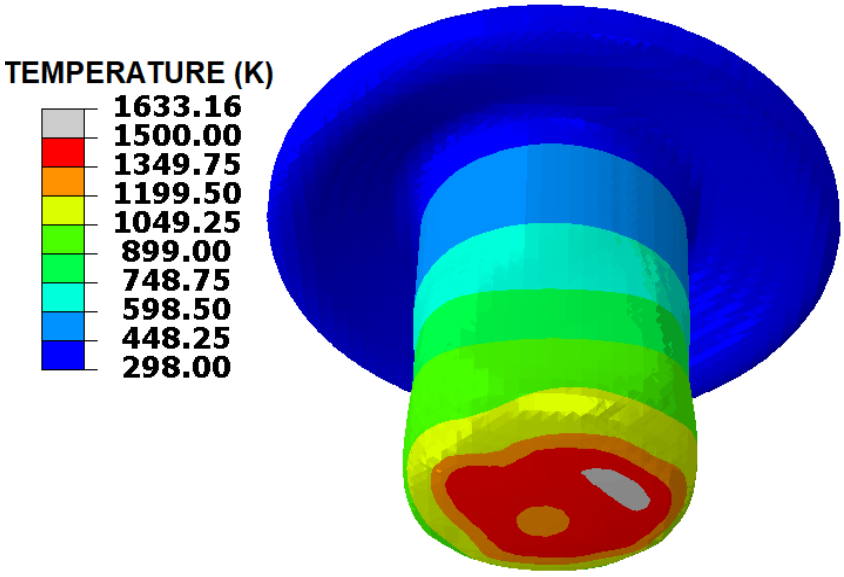
TEMPERATURE (K)
1633.16
1500.00
1349.75
1199.50
1049.25
899.00
748.75
598.50
448.25
298.00

(B)

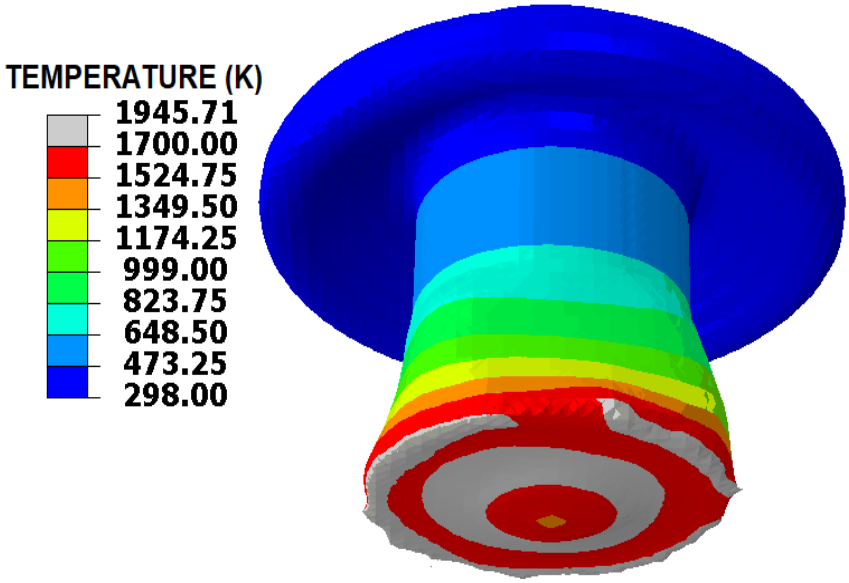
TEMPERATURE (K)
1945.71
1700.00
1524.75
1349.50
1174.25
999.00
823.75
648.50
473.25
298.00

(C)

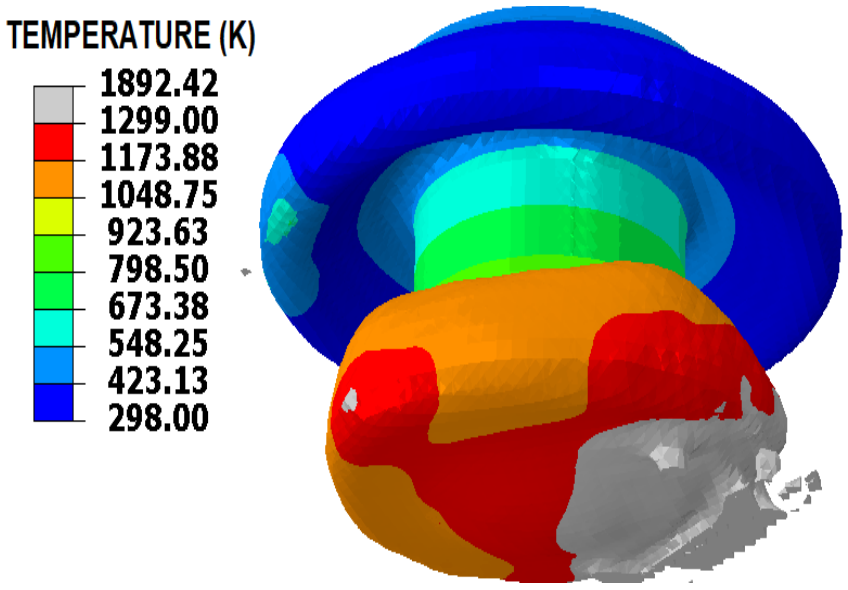

(D)

FIGURE 27 FRONT VIEW OF FRICTION ELEMENT, TEMPERATURE DISTRIBUTION AT END OF (A) PENETRATION (B) CLEANING (C) WELDING AND (D) COMPRESSION

4.3. Effect of Endload & Rotational Speed:

With the objective of analyzing the effect of varying rotational feed and endload on the amount of heat generated, plastic deformation, and the subsequent weld quality, three different sets of process parameters namely, Set-2, Set-3, and Set-4 were tested. Set-3 and Set-4 are shown in TABLES 11 and 12 respectively whereas Set-2 has the same parameters as mentioned in Table 8.

TABLE 11 PROCESS PARAMETERS FOR SET-3

Step	Feed velocity (mm/s)	Rotational speed (RPM)	Time (s)
penetration	9.42	5000	0.138
cleaning	1.39	6000	0.576
welding	7.86	4000	0.14
compression	2	0	0.322

TABLE 12 PROCESS PARAMETERS FOR SET-4

Step	Feed velocity (mm/s)	Rotational speed (RPM)	Time (s)
penetration	8.61	5000	0.151
cleaning	1.51	6000	0.796
welding	24.14	6000	0.029
compression	2	0	0.313

Three different Points were selected on each part, i.e. two layers of workpiece and the friction element, for the purpose of temperature evolution study as shown in FIGURE 28. Points-A, B, and C are located at bottom surface of aluminum layer at distances of 0.9 mm, 3.16 mm, and 5 mm respectively from the element center. For the steel layer, Points-D, E, and F located at its top surface at distances of 1.22 mm, 2.44 mm, and 3.66 mm were

selected whereas for the friction element, Points-G, H, and I were selected wherein ‘G’ is present near the bottom of the element and ‘H’ and ‘I’ are present at distances of 1.6 mm and 3.3 mm respectively. All the Points were selected with the aim of showing the extent of heat dissipation and temperature reached at these locations within different parts and how they evolve under different process parameters. Temperature measurements from Sets-2, 3, and 4 at these Points are presented in FIGURES 29, 30, and 31.

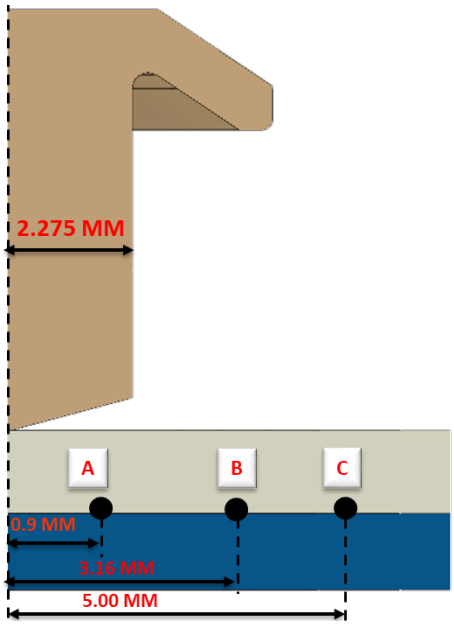

(A)

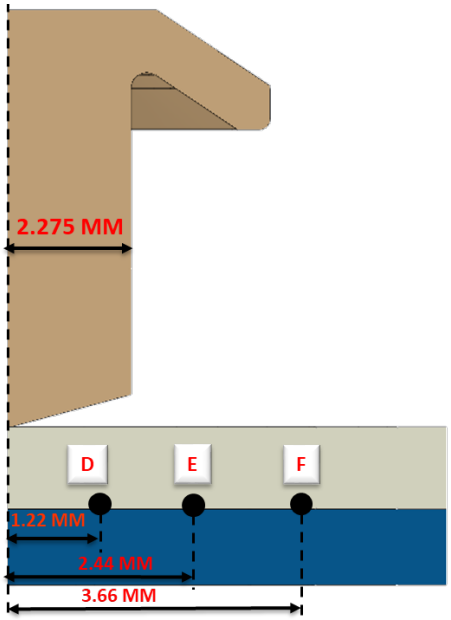

(B)

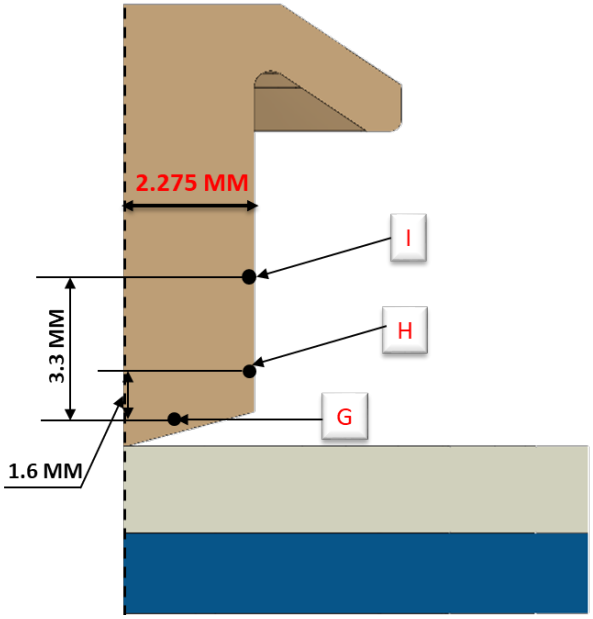

(C)

FIGURE 28 NODAL POINTS CHOSEN FOR TEMPERATURE EVOLUTION IN (A) TOP LAYER (B) BOTTOM LAYER AND (C) FRICTION ELEMENT

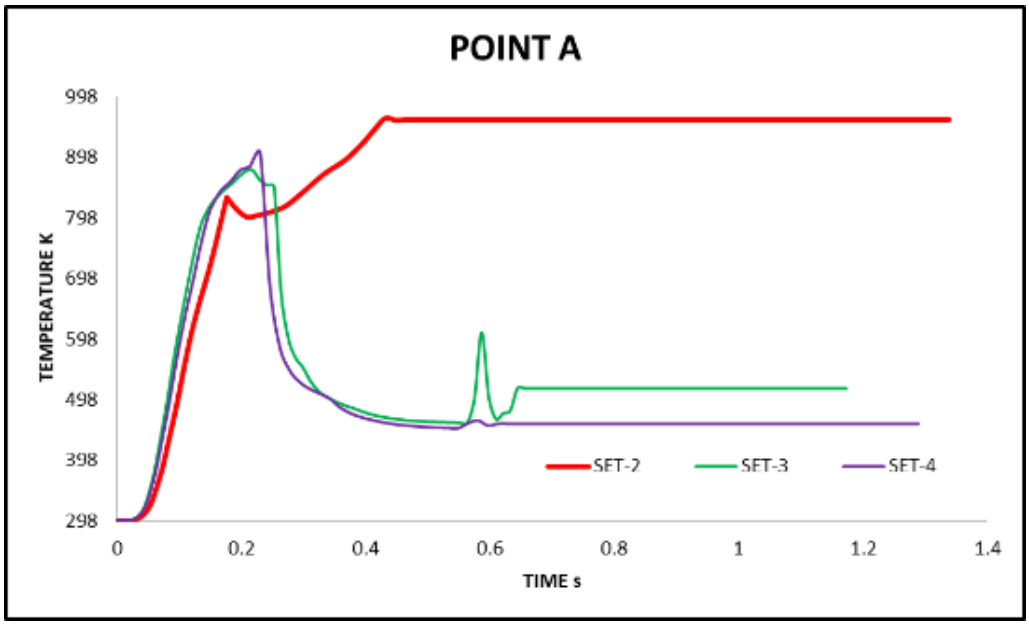
POINT A
998
898
798
698
598
498
398
298
TEMPERATURE K
0
0.2
0.4
0.6
0.8
1
1.2
1.4
TIME s
SFT-2
SFT-3
SFT-4

(A)

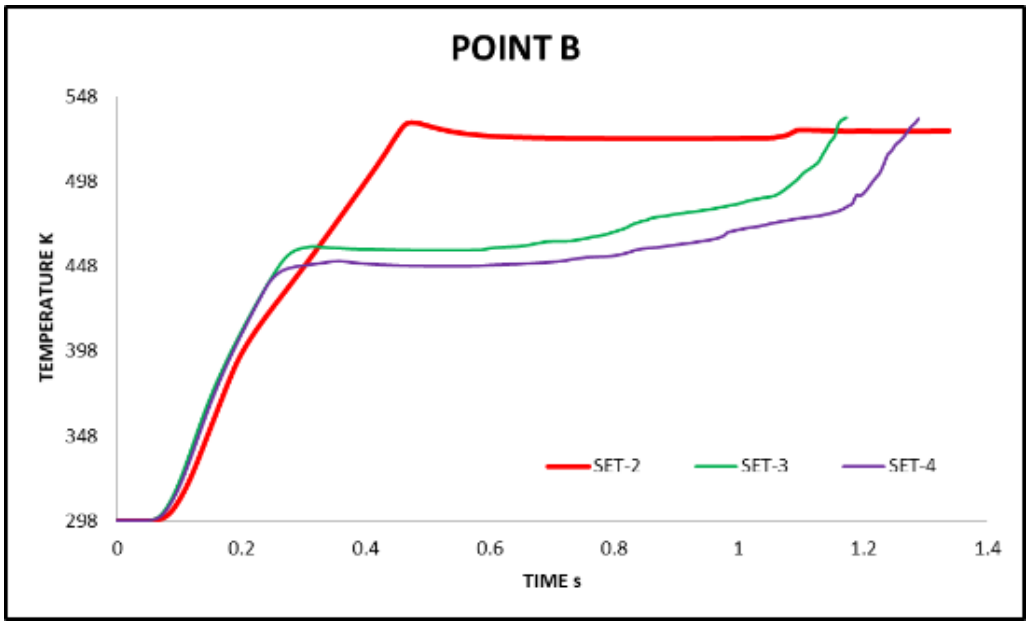
POINT B
548
498
448
398
348
298
TEMPERATURE K
0
0.2
0.4
0.6
0.8
1
1.2
1.4
TIME s
SFT-2
SFT-3
SFT-4

(B)

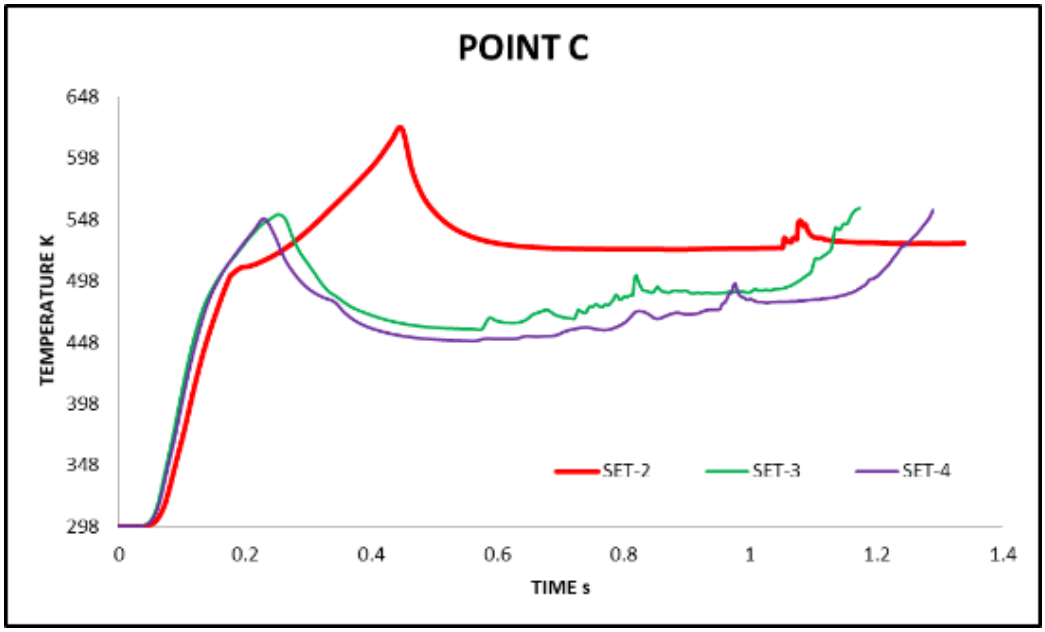

(C)

FIGURE 29 TEMPERATURE EVOLUTION AT POINTS- A, B, AND C IN ALUMINUM LAYER IN FIGURE 28(A)

The temperature evolution of Points-A, B, and C chosen in top aluminum layer is shown in FIGURE 29. A distinct pattern emerges at all the three locations i.e. Set-2 reaches the highest peak of temperature whereas Sets-3, 4 have approximately the similar temperature values. For the same rotational speed, Set-2 has the longest Penetration step which allows for higher period of friction interaction between the element and aluminum layer leading to more heat generation and higher temperature in the aluminum layer. For Cleaning and Welding, the temperature remains at a relatively steady state but as the element makes contact with the steel layer, the temperature in Sets-3, 4 increases during

end of Welding due to friction heat generation between the interacting parts. Under the application of high endload in Compression, heat transfer from both the steel parts results in a rise in temperature at Points-B, C for Sets-3, 4. Due to the lowest rotational speed in Cleaning and Welding, a drop in temperature at Point-C for Set-2 is observed indicating that the amount of heat generated is highly influenced by the rotational speed of the element. Unlike in the case of Sets-3, 4, the temperature at different Points for Set-2 tends to remain steady and does not increase as the element rotates at a relatively constant speed, which is lower than other sets, for major portion of FEW process. The drop in temperature followed by a steady state for Point-A is an indicator of elements being deleted as they are subjected to deformation under the rotating friction element.

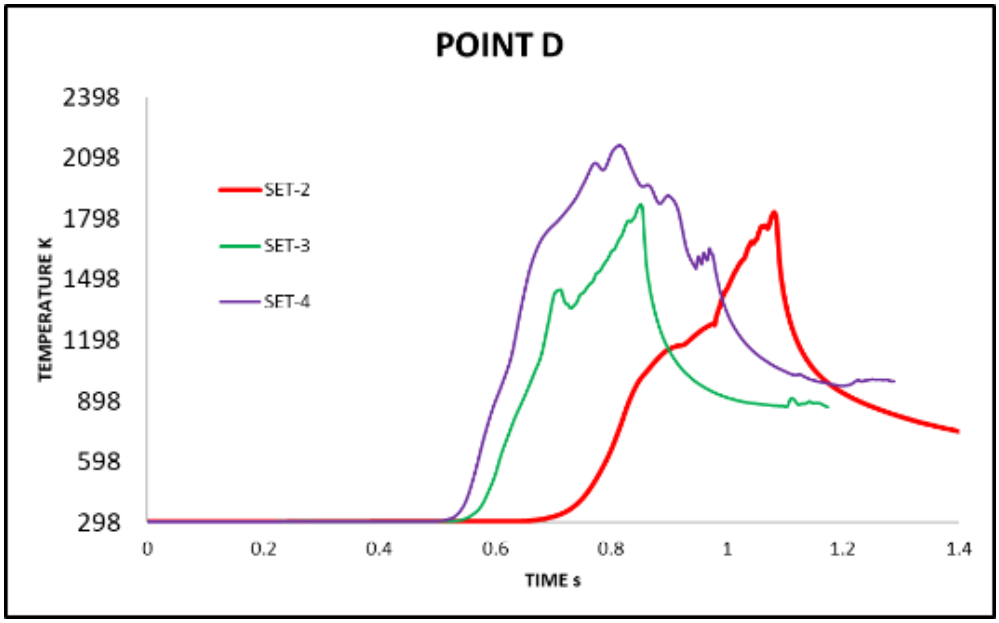

(A)

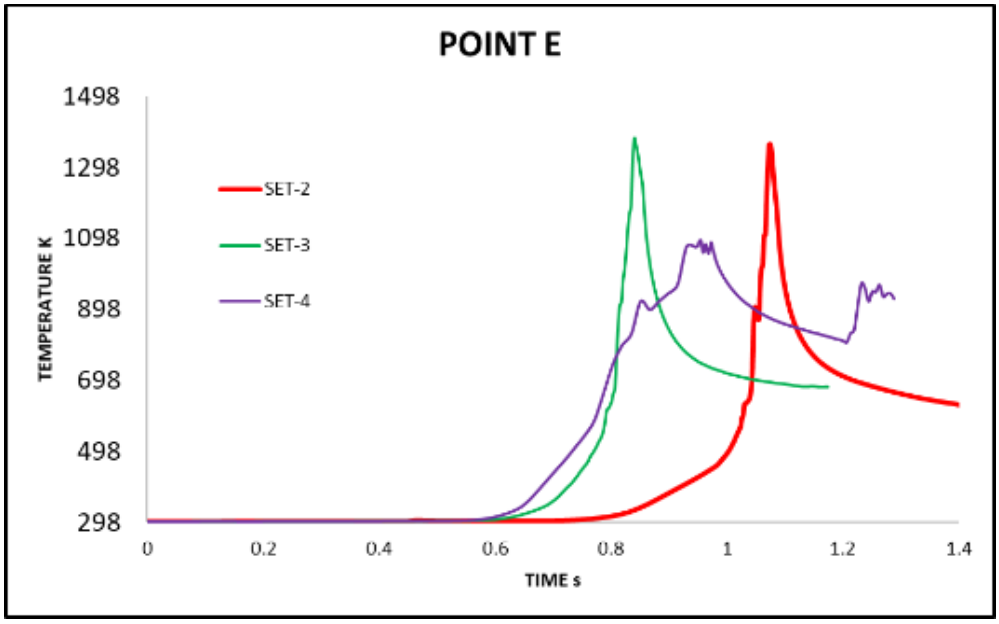

(B)

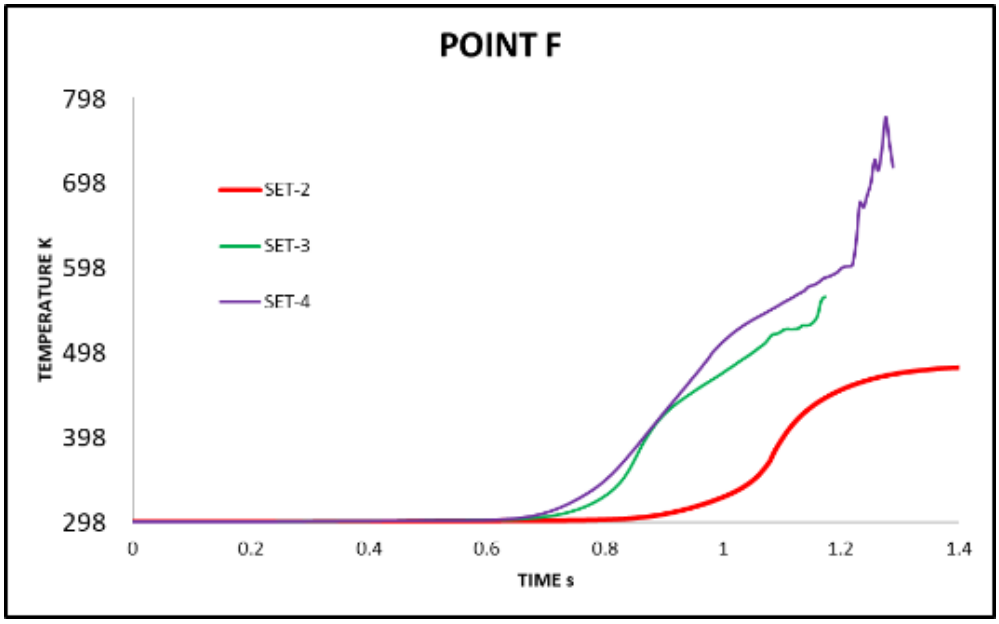

(C)

FIGURE 30 TEMPERATURE EVOLUTION AT POINTS- D, E, AND F IN STEEL LAYER IN FIGURE 28(B)

Different points selected for the evaluation of temperature variation in the steel layer can be seen in FIGURE 30 wherein for all the locations, room temperature prevails until the friction element makes contact with the steel layer after drilling through aluminum layer. For the three points selected, the rise in temperature in steel layer is observed at a much later time point for Set-2 when compared to Sets-3, 4 due to longer Penetration step which results in more heat generation at aluminum layer-element interface. Although Set-2 has the highest endload and step time specified during Cleaning and second highest step time during Welding, due to the lowest rotational speed the amount of heat generated in it is significantly lower than that those in Sets-3, and 4. As a result, temperature magnitude is observed to be the lowest for Set-2. For point-D, Set-4 has the highest peak temperature which can be attributed to the long Cleaning step time as well as high rotational speed which allows for longer duration for friction interaction between the steel-steel parts resulting in large amount of heat generation. At the same location, for the same endload and rotational speed as that of Set-4, the heat generated in Set-3 is much lower, due to the smaller Cleaning step which indicates inadequate time for heat conduction into the steel layer. Set-2 has the lowest peak temperature although its Cleaning step time is the longest but due to its lowest rotational speed, not enough friction heat generation occurs at the steel-steel interface leading to lower temperatures. The difference between the peak values of Set-2 and Set-4 at point-D is about 550 K indicating the effect rotational speed has on the heat generation. For point-E, Sets-2, 3 have similar peak temperatures at about 1300 K much higher than the peak temperature of 1050 K for Set-4 which is a consequence of longer Welding steps, allowing sufficient time for propagation of the heat generated at the

top surface into the steel layer. However, the time point at which the peak values are reached differ significantly. The peak value for Set-3 (higher rotation and lower endload) is reached at about 0.84 s whereas for Set-2 (lower rotation and higher endload), the time taken to reach peak value is about 1.07 s, which means that the total process time would be higher for Set-2 to achieve the desired deformation in the element. Point F which is at a distance of 3.66 mm represents the extent of heat conduction within the steel layer. As observed at other points higher rotational speed results in higher frictional heat generation and as such, Sets-3, 4 have higher magnitude than Set-2 which has the lowest rotational speed. The peak value reached is the highest for Set-4 at about 680 K followed by Set-3 at 560 K and lastly, at 480 K for Set-2. For a point away from the interaction region, a difference of 200 K in temperature for Set-2 and Set-4 implies that longer Cleaning and Welding steps with higher endload does not translate into higher friction heat generation without the presence of adequate rotational speed.

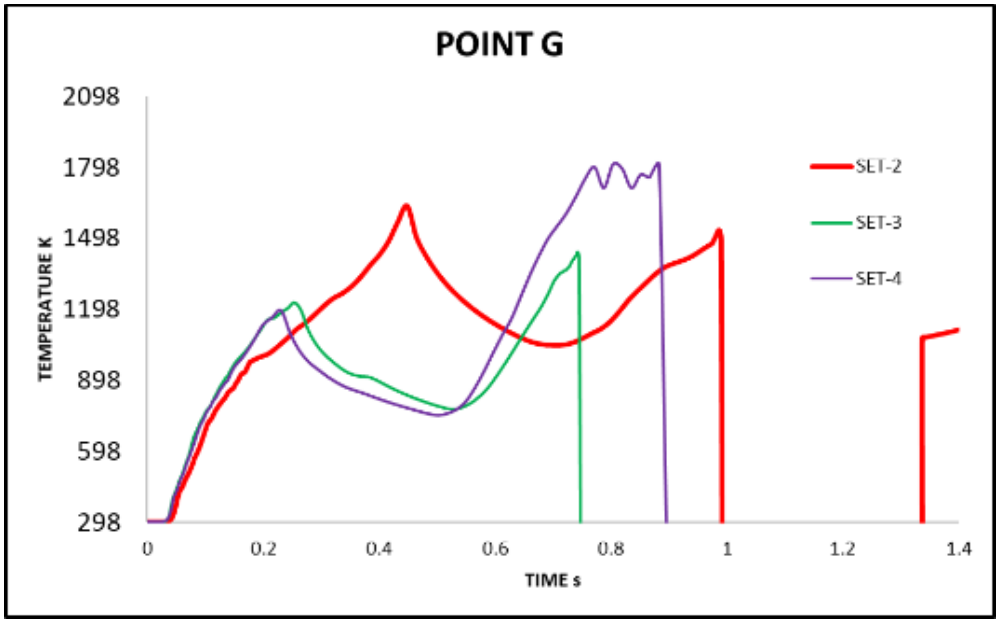
POINT G
2098
1798
1498
1198
898
598
298
TEMPERATURE K
0
0.2
0.4
0.6
0.8
1
1.2
1.4
TIME s
SET-2
SET-3
SET-4

(A)

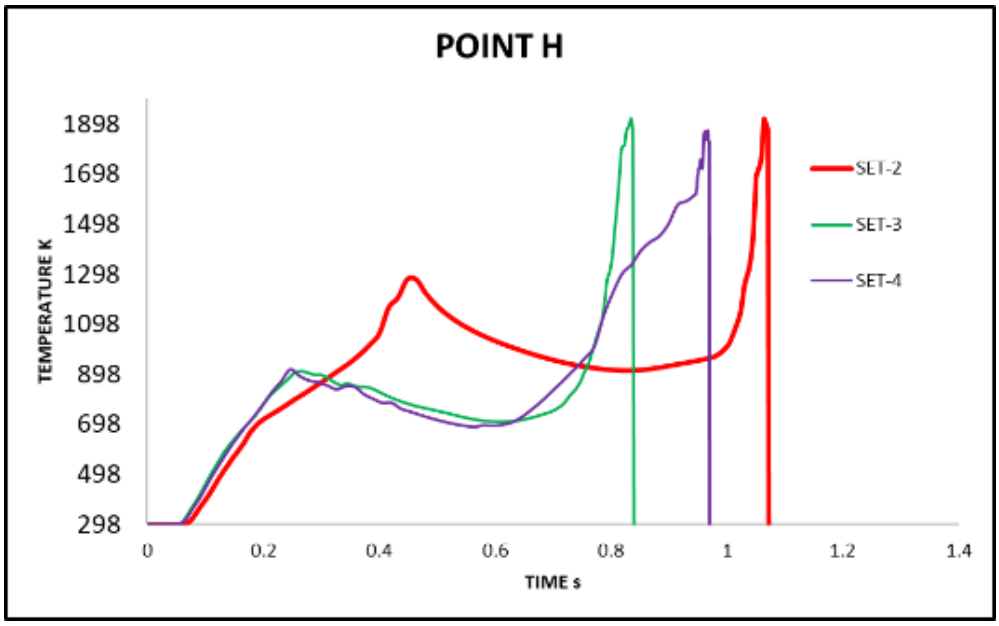
POINT H
1898
1698
1498
1298
1098
898
698
498
298
TEMPERATURE K
0
0.2
0.4
0.6
0.8
1
1.2
1.4
TIME s
SET-2
SET-3
SET-4

(B)

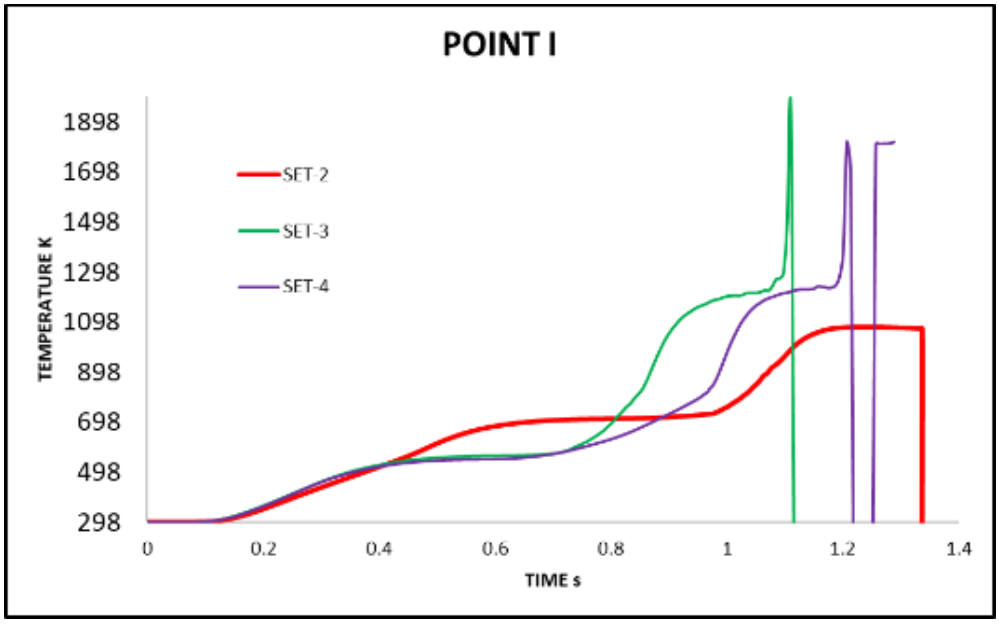

(C)

FIGURE 31 TEMPERATURE EVOLUTION AT POINTS- G, H, AND I IN FRICTION ELEMENT IN FIGURE 28(C)

To understand how temperature evolves under different processing conditions, three Points- G, H, and I were selected within the friction element as shown in FIGURE 28(C). Point G is located near the bottom region of the element whereas Points 'H', 'I' are located at distances of 1.6 mm and 3.3 mm respectively from point G. Due to the Eulerian nature of the friction element, material continuously moves within the rigid Eulerian framework thereby some elements will be partially/completely empty at varying time Points resulting in drop in temperature as observed in FIGURE 31. It can be seen that for Points-G, H there are two instances at which peak values of temperature are obtained, the first one occurring during Cleaning and the second one occurring during Welding. The

reason for existence of two peaks is due to the fact that friction element continuously generates heat by interacting with aluminum layer until element deletion starts and thereafter, it comes into contact with colder steel layer resulting in loss of heat and lower friction heat generation. At Point-G which is the nearest to the friction interaction region in the element, the first peak value of temperature occurs much earlier for Sets-3, 4 than in the case of Set-2. Also, the magnitude of the first peak for Sets-3, 4 is approximately identical at 1200 K whereas in the case of Set-2 the peak value is observed to be above 1600 K. The significant difference between the magnitudes of the first peak as well as the time point at which they are reached is a direct consequence of longer Penetration step time while other parameters being the same which aids in stronger heat generation at the interface of harder friction element-softer aluminum layer. As sufficient heat is generated at the interface and temperature of aluminum layer rises to near its melting point, its thermal conductivity decreases sharply. It deforms significantly under the applied endload thereby allowing for greater heat transfer into the element than into itself. Further into the process after the first peak, a drop in the element temperature is observed as it contacts the relatively colder steel layer and it continues to decrease until enough heat generation occurs by friction interaction between the two parts. It must be noted that even by the end of Cleaning step, the shape of friction element is well maintained even though temperature rises above 1350 K in different sets. Due to the high hardness at elevated temperatures and ample time for friction interaction i.e. long Cleaning step, the second peak for Set-4 reaches a value of 1810 K, well above its melting temperature. If we consider the case of Set-2 which also had the same characteristics of hardness and long Cleaning step the second peak value for

it is observed to be at 1500 K, much lower than the peak for Set-4. The primary reason behind this significant gap in the friction heat generation and subsequent temperature values is the lower rotational speed of the friction element in Set-2. With respect to Set-3 which has the shortest Cleaning step but the highest rotational speed, the longest Welding step with the lowest rotational speed, the second peak value at 1420 K is observed to be only slightly lower than that of Set-2. As we move further up the friction element at point H, the evolution trend is similar to that observed at point G i.e. two different peaks, one during Cleaning and the other during Welding with the first peak at 1260 K for Set-2 and reaching at a later time point than that of Sets-3, 4 which have the same first peak value at 890 K. After the first peak, a steady decrease in the element temperature is followed by a sharp increase in temperature. The same phenomenon was observed at point G and the reasons attributed, i.e. lower rotational speed and varying step time for this particular phenomena apply to point H as well. However, the values of the second peak for the three different sets are within a close range of 1850 K to 1900 K and it occurs near the end of Welding. The occurrence of the second peak values within such a close range is an indication that deformation is highly localized and does not takes place far away from the bottom portion even when such high temperatures are reached by end of the Welding. The instantaneous drop observed at the start of Compression is an outcome of significant material movement within the Eulerian mesh under the increased endload. When we consider the point I located 3.3 mm away from bottom region, a single peak value for each set is observed which is during the Compression step. As the applied endload increases by a high amount in the Compression step, the heated friction element undergoes high amount

of localized plastic deformation near the bottom region which tends to displace the material laterally as well as in the upward direction. This movement of heated material in the Eulerian friction element, carries away the heat from the friction interaction region to locations farther away from it resulting in temperatures as high as 1200 K (at point I). Due to the high hardness and ability to retain it during elevated temperatures, the plastic deformation is concentrated near the bottom region which ultimately promotes a mechanical locking between the two layers and the element as well as a weld formation between the heated bottom portion of the element and the top surface of steel layer.

CHAPTER FIVE
CONCLUSIONS AND FUTURE WORK

5.1. Conclusions:

The current research work has presented a new methodology for successfully simulating processes which are marked by the presence of high degree of deformation and temperature variations without experiencing any pre-mature or abrupt ending of the calculations due to any mesh related issues. Using the coupled Eulerian-Lagrangian scheme, the author has been able to simulate the friction element welding process in its entirety with coupling of thermal and mechanical equations. The FEM results were found to be in good agreement with experimental results with respect to the plastic deformation as well as the temperature measurements at multiple locations. The severe deformation of the friction element as well as that of the two layers of workpiece was captured very well by the FEM.

5.2. Intellectual Merit:

The distinguishing feature of FEW process is the very high magnitude of plastic deformation of the friction element which is not present in other similar friction based joining processes. The deformation of friction element is a critical aspect from the point of view of weld quality and it is effected by multiple factors such as rotational speed, endload, etc. Experimentally, it is extremely difficult to monitor the transient interactions taking place within the weld zone thereby mandating the requirement of a numerical model which

would help reveal the different mechanisms taking place during the process. Another aspect which has to be regarded is the inter-dependency of mechanical behavior on thermal conditions and vice-versa. Without including this inter-dependency, an accurate simulation of the FEW process is unachievable. This further adds to the already complex FEM making it even more difficult to obtain a satisfying solution within a practical time period.

Developing a finite element model which can capture deformation of this degree while also performing thermal calculations makes it a highly difficult task. To the best of author's knowledge, the use of Eulerian definition for a tool is first of its kind in the domain of simulating friction joining processes. The scheme of coupled Eulerian-Lagrangian used in the current research work was able to yield satisfactory results which matched well with experimental observations. The successful implementation of this unique scheme would aid fellow researchers in broadening their resources in meeting their goal of achieving a coupled thermal-mechanical FEM void of distortion issues, for highly transient process involving high levels of plastic deformation. Moreover, the developed finite element model was able to complete the numerical calculations within a practical timeline of 36 to 72 hours depending on the mesh density and total process time which makes it a highly lucrative alternative to the time & efforts consuming experimentation for the purpose of analysis and optimization.

5.3. FEM of Friction Element Welding:

Using the validated finite element model, analysis could be carried out with respect to the various interactions and their eventual effects on the thermal and mechanical properties of different parts. It was observed that the temperature rise in the top aluminum layer occurs during Penetration and the first half of Cleaning. It then remains steady until the start of Compression, after which an increase in temperature is observed due to high material movement in the interaction region. Due to the absence of thermal conductance between the two layers of workpiece, the temperature of the steel layer remains at room temperature until the friction element interacts with it, following which there is substantial increase in the steel layer temperature. When the element contacts the steel layer, there is temperature drop in the element due to low friction heat generation between the heated element and cold steel layer. With increase in the temperature of the steel layer, the amount of friction interaction increases as well and reaches a peak value. After which, friction interaction decreases rapidly due to heat dissipation in the Compression stage. The peak of temperatures reached in the friction element and the steel layer are very close to their respective melting temperatures indicating the high heat generation due to friction interaction and plastic deformation of different parts. Also, the heated area is confined to a very small region slightly larger than the diameter of friction element. The friction element tends to maintain its structural integrity through Cleaning due to its high hot hardness. But as the friction interaction reaches a peak value in the Welding, it is heated sufficiently to initiate the deformation. Finally, the application of high endload in the Compression step

furthers the degree of localized plastic deformation, thus forming the required weld between the two layers and the element.

5.4. Effect of Variation of Process Parameters:

The primary parameters found to be having significant influence on the heat generation and subsequent weld quality are the rotational speed of the friction element and the endload applied on it. Using three different sets of process parameters with varying rotational speed, endload, and step time, their effect on the heat generation and subsequent temperatures in different parts have been analyzed. It was found that for a set with longer Penetration step and high element rotation, higher heat generation occurs at the aluminum layer-steel element interface. The major portion of this generated heat is transferred into aluminum layer resulting in high levels of temperature but lower than its melting point. For a set with longer Cleaning step but with lower rotational speed and higher endload, the amount of friction heat generation is drastically lower than the set with similar Cleaning step time, higher rotational speed and lower endload. The time period of Welding step can be increased or decreased by modifying the rotational speed and endload accordingly so as to achieve the required amount of friction heat generation to ensure that the bottom portion of element is heated enough to induce deformation in the final step. The amount of deformation undergone by the two layers and the friction element is primarily dependent on the amount of heat generated during the friction interaction which is again influenced by the rotational speed of the element and the amount of time given for steel-steel parts

interaction. For achieving such high deformation of the hard friction element, the temperatures in the interaction region are required to reach near their melting temperatures, devoid of which higher endloads are required.

5.5. Future Work:

The current finite element model can be improved further by including gap thermal conductance between the two layers, employing a temperature dependent friction coefficient, and varying the shear stress limit in accordance with the prevailing temperature to better depict the real conditions and interactions of the FEW process. Another area of improvement would be in modifying (read increasing) the mesh density of different parts while not increasing the total compute time.

The results from the simulation can help identify regions which have experienced high deformation and also have high level of temperatures at different time points in the FEW process. This information can be used in conducting microstructural analysis to investigate for any changes in the phase or find any evidence of diffusion of materials in the weld and nearby zones. The effect of the coating layer present on the workpiece materials is still unknown. Its role in the weld formation and providing strength can be made clear by studying the microstructural evolution of the weld zone at different points. This would help better understand the fundamental joining mechanisms of the FEW process.

The current research work has simulated welding of sheets which have maximum thickness of 1.5 mm, however the requirements of automotive industry vary beyond this thickness and to efficiently weld such thick sheets would require considerable amount of heat energy to plasticize the materials. Generating such high levels of heat using just the friction element would make FEW process infeasible in such cases and it also loses out on the advantage of low time consumption. This gap can be addressed by infusing an auxiliary source of energy like a laser beam and thus, supplying sufficient energy to complete a good quality in desirable time period. Future work would include exploring the possibilities of inclusion of secondary energy sources to fasten the process in joining of thick sheets of dissimilar materials.

REFERENCES

[1] Kah, P., Suoranta, R., Martikainen, J., and Magnus, C., 2014, "Techniques for Joining Dissimilar Materials : Metals and Polymers," **36**(April), pp. 152–164.

[2] Messler, R. W., "PRINCIPLES OF ."

[3] Weman, K., 2003, *Welding Processes Handbook*.

[4] "EAA Aluminium Automotive Manual – Joining," pp. 1–31.

[5] Pervaiz, M., 2016, "Emerging Trends in Automotive Lightweighting through Novel Composite Materials Emerging Trends in Automotive Lightweighting through Novel Composite Materials," (March).

[6] Gould, J. E., 2012, "Joining Aluminum Sheet in the Automotive Industry – A 30 Year History," Weld. J., **91**, pp. 23–34.

[7] Isenstadt, A., German, J., Bubna, P., Wiseman, M., Venkatakrishnan, U., Abbasov, L., Guillen, P., Moroz, N., Richman, D., and Kolwich, G., 2016, "Lightweighting Technology Development and Trends in U.S. Passenger Vehicles," p. 24.

[8] Correia, J. R., and Soares, C. M. M., 2015, "10th International Conference on Composite Science and Technology ICCST/10."

[9] Belingardi, G., 2014, "Lightweight Design of Vehicle Body a Contribution Toward Greener Environment," ACTA Teh. Corviniensis - Bull. Eng., **7**(1), pp. 49–54.

[10] Taub, A. I., and Luo, A. A., 2015, "Advanced Lightweight Materials and Manufacturing Processes for Automotive Applications," MRS Bull., **40**(12), pp. 1045–1053.

[11] "No Title" [Online]. Available: http://articles.sae.org/15545/.

[12] Hong, K.-M., and Shin, Y. C., 2017, "Prospects of Laser Welding Technology in the Automotive Industry: A Review," J. Mater. Process. Technol., **245**, pp. 46–69.

[13] Miller, W. ., Zhuang, L., Bottema, J., Wittebrood, A. ., De Smet, P., Haszler, A., and Vieregge, A., 2000, "Recent Development in Aluminium Alloys for the Automotive Industry," Mater. Sci. Eng. A, **280**(1), pp. 37–49.

[14] "No Title."

[15] Taban, E., Gould, J. E., and Lippold, J. C., 2010, "Dissimilar Friction Welding of 6061-T6 Aluminum and AISI 1018 Steel: Properties and Microstructural Characterization," Mater. Des., **31**(5), pp. 2305–2311.

[16] Mucha, J., 2017, "Clinching Technology in the Automotive Industry," Automot. Arch., **76**(2), pp. 75–94.

[17] Michalos, G., Makris, S., Papakostas, N., Mourtzis, D., and Chryssolouris, G., 2010, "Automotive Assembly Technologies Review: Challenges and Outlook for a Flexible and Adaptive Approach," CIRP J. Manuf. Sci. Technol., **2**(2), pp. 81–91.

[18] Lazarevic, S., Miller, S. F., Li, J., and Carlson, B. E., 2013, "Experimental Analysis of Friction Stir Forming for Dissimilar Material Joining Application," J. Manuf. Process., **15**(4), pp. 616–624.

[19] Ratanathavorn, W., “Hybrid Joining of Aluminum to Thermoplastics with Friction Stir Welding Master of Science Thesis by Department of Materials Science and Engineering.”

[20] Ma, C., and Lan, F., 2015, “Review the Research Trends and Application in Car Body of Aluminum Foam *,” **729**, pp. 73–78.

[21] Martinsen, K., Hu, S. J., and Carlson, B. E., 2015, “Joining of Dissimilar Materials,” CIRP Ann. - Manuf. Technol., **64**(2), pp. 679–699.

[22] Barnes, T. ., and Pashby, I. ., 2000, “Joining Techniques for Aluminium Spaceframes Used in Automobiles,” J. Mater. Process. Technol., **99**(1–3), pp. 62–71.

[23] Khomenko, A., 2015, “Composite, Hybrid, and Multifunctional Materials, Volume 4,” (June).

[24] Das, S., Graziano, D., Upadhyayula, V. K. K., Masanet, E., Riddle, M., and Cresko, J., 2016, “Vehicle Lightweighting Energy Use Impacts in U.S. Light-Duty Vehicle Fleet,” Sustain. Mater. Technol., **8**, pp. 5–13.

[25] Prangnell, P., Haddadi, F., Chen, Y. C., Prangnell, P., and Chen, F. H. C., 2017, “Ultrasonic Spot Welding of Aluminium to Steel for Automotive Applications — Microstructure and Optimisation Ultrasonic Spot Welding of Aluminium to Steel for Automotive Applications Microstructure and Optimisation,” **0836**(July).

[26] Feng, Z., Santella, M. L., David, S. A., Steel, R. J., Packer, S. M., Pan, T., Kuo, M., and Bhatnagar, R. S., 2005, “Friction Stir Spot Welding of Advanced High-Strength Steels - A Feasibility Study,” (January).

[27] Dong, H., Chen, S., Song, Y., Guo, X., Zhang, X., and Sun, Z., 2016, “Refilled Friction Stir Spot Welding of Aluminum Alloy to Galvanized Steel Sheets,” Mater. Des., **94**, pp. 457–466.

[28] Eshtayeh, M. M., Hrairi, M., and Mohiuddin, A. K. M., 2016, “Clinching Process for Joining Dissimilar Materials: State of the Art,” Int. J. Adv. Manuf. Technol., **82**(1–4), pp. 179–195.

[29] Meschut, G., Janzen, V., and Olfermann, T., 2014, “Innovative and Highly Productive Joining Technologies for Multi-Material Lightweight Car Body Structures,” J. Mater. Eng. Perform., **23**(5), pp. 1515–1523.

[30] Mori, K., Abe, Y., and Kato, T., 2014, “Self-Pierce Riveting of Multiple Steel and Aluminium Alloy Sheets,” J. Mater. Process. Technol., **214**(10), pp. 2002–2008.

[31] Li, D., Chrysanthou, A., Patel, I., and Williams, G., 2017, “Self-Piercing Riveting-a Review,” Int. J. Adv. Manuf. Technol., **92**(5–8), pp. 1777–1824.

[32] Roca, S. F., and Cited, R., 2006, “(12) United States Patent,” **2**(12).

[33] Skovron, J. D., Ruszkiewicz, B. J., Mears, L., Abke, T., Varma, A., Li, Y., Choi, H., and Zhao, X., 2017, “Investigation of the Cleaning & Welding Steps from the Friction Element Welding Process,” *ASME 2017 12th International Manufacturing Science and Engineering Conference, MSEC 2017 Collocated with the JSME/ASME 2017 6th International Conference on Materials and Processing*.

[34] Schubert, H., and Möhring, J., 2012, “Flexible Material Joining Technology for

Tomorrow ` s Innovative Lightweight Design Today ´ s Challenges in Automobil Production."

[35] Gmbh, E., 2015, "EJOT ® The Quality Connection Business Unit EJOWELD ® Composite D Esign „ Made E Asy "."

[36] Meschut, G., Hahn, O., Janzen, V., and Olfermann, T., 2014, "Innovative Joining Technologies for Multi-Material Structures," Weld. World, **58**(1), pp. 65–75.

[37] Meshing, A., Adaptive, L., Domains, M., Adaptive, E., Domains, M., Analyses, S., Features, A., Meshing, A., and Control, E. D., 2005, "Adaptive Meshing and Distortion Control."

[38] Oliphant, A., 2004, "Numerical Modeling of Friction Stir Welding: A Comparison of Alegra and Forge3," (August), pp. 3–5.

[39] Gakwaya, A., Sharifi, H., Guillot, M., Souli, M., and Erchiqui, F., 2011, "ALE Formulation and Simulation Techniques in Integrated Computer Aided Design and Engineering System with Industrial Metal Forming Applications," **73**(3), pp. 209–266.

[40] Johnson, G. R., and Cook, W. H., 1985, "Fracture Characteristics of Three Metals Subjected to Various Strains, Strain Rates, Temperatures and Pressures," Eng. Fract. Mech., **21**(1), pp. 31–48.

[41] Alitavoli, M., Darvizeh, A., Moghaddam, M., Parghou, P., and Rajabiehfard, R., 2018, "Numerical Modeling Based on Coupled Eulerian-Lagrangian Approach and Experimental Investigation of Water Jet Spot Welding Process," Thin-Walled Struct., **127**(February), pp. 617–628.

[42] Grujicic, M., Snipes, J. S., and Ramaswami, S., 2017, "Process Modeling , Joint Virtual Testing and Construction of Joint Connectors for Mechanical Fastening by Flow-Drilling Screws," **231**(6), pp. 1048–1061.

[43] Atharifar, H., Lin, D., and Kovacevic, R., 2009, "Numerical and Experimental Investigations on the Loads Carried by the Tool during Friction Stir Welding," J. Mater. Eng. Perform., **18**(4), pp. 339–350.

[44] Kim, D., Badarinarayan, H., Kim, J. H., Kim, C., Okamoto, K., Wagoner, R. H., and Chung, K., 2010, "Numerical Simulation of Friction Stir Butt Welding Process for AA5083-H18 Sheets," Eur. J. Mech. A/Solids, **29**(2), pp. 204–215.

[45] Reilly, A., Shercliff, H., Chen, Y., and Prangnell, P., 2015, "Journal of Materials Processing Technology Modelling and Visualisation of Material Flow in Friction Stir Spot Welding," J. Mater. Process. Tech., **225**, pp. 473–484.

[46] Schmidt, H., and Hattel, J., 2005, "A Local Model for the Thermomechanical Conditions in Friction Stir Welding," Model. Simul. Mater. Sci. Eng., **13**(1), pp. 77–93.

[47] Schwer, L. E., 2009, "ALUMINUM PLATE PERFORATION : A COMPARATIVE CASE STUDY USING LAGRANGE with EROSION , MULTI-MATERIAL ALE , and SMOOTH PARTICLE HYDRODYNAMICS."

[48] Mastin, L. G., 2002, "Numerical Model," **4**(2), p. 80.

[49] Nourani, M., 2013, "Integrated Multiphysics Modeling , Testing and Optimization

of Friction Stir Welding of Aluminum," (October), p. 205.

[50] Hirasawa, S., Badarinarayan, H., Okamoto, K., Tomimura, T., Kawanami, T., and Hirano, S., 2009, "Analysis of Temperature and Plastic Flow during Friction Stir Spot Welding Using Particle Method," J. Therm. Sci. Technol., **4**(2), pp. 260–271.

[51] Yang, H., Yang, H., and Hu, X., 2015, "Simulation on the Plunge Stage in Refill Friction Stir Spot Welding of Aluminum Alloys," (ICMMCCE), pp. 521–524.

[52] Reilly, A., and Meng, M. A., 2013, "Modelling of Friction Stir Spot Welding," (May).

[53] Weinberger, T., and Enzinger, N., 2010, "THERMO-MECHANICAL INVESTIGATIONS DURING FRICTION STIR SPOT WELDING (FSSW) OF AA6082-T6," pp. 134–146.

[54] Awang, M., and Mucino, V. H., 2006, "Thermo-Mechanical Modeling of Friction Stir Spot Welding (FSSW)," Engineering, (724), pp. 1–6.

[55] Jedrasiak, P., Shercliff, H. R., Reilly, A., McShane, G. J., Chen, Y. C., Wang, L., Robson, J., and Prangnell, P., 2016, "Thermal Modeling of Al-Al and Al-Steel Friction Stir Spot Welding," J. Mater. Eng. Perform., **25**(9), pp. 4089–4098.

[56] Kim, D., Badarinarayan, H., Ryu, I., Kim, J. H., Kim, C., Okamoto, K., Wagoner, R. H., and Chung, K., 2010, "Numerical Simulation of Friction Stir Spot Welding Process for Aluminum Alloys," Met. Mater. Int., **16**(2), pp. 323–332.

[57] Muci-Küchler, K. H., Kalagara, S., and Arbegast, W. J., 2010, "Simulation of a Refill Friction Stir Spot Welding Process Using a Fully Coupled Thermo-Mechanical FEM Model," J. Manuf. Sci. Eng., **132**(1), p. 014503.

[58] Khosa, S. U., Weinberger, T., and Enzinger, N., 2010, "Thermo-Mechanical Investigations during Friction Stir Spot Welding (FSSW) of AA6082-T6," Weld. World, **54**(5–6).

[59] Nandan, R., Roy, G. G., and Debroy, T., 2006, "Numerical Simulation of Three-Dimensional Heat Transfer and Plastic Flow during Friction Stir Welding," Metall. Mater. Trans. A, **37**(4), pp. 1247–1259.

[60] Mandal, S., Rice, J., and Elmustafa, A. A., 2008, "Experimental and Numerical Investigation of the Plunge Stage in Friction Stir Welding," J. Mater. Process. Technol., **203**(1–3), pp. 411–419.

[61] Ulysse, P., 2002, "Three-Dimensional Modeling of the Friction Stir-Welding Process," **42**(June), pp. 1549–1557.

[62] Su, H., Wu, C. S., Bachmann, M., and Rethmeier, M., 2015, "Numerical Modeling for the Effect of Pin Profiles on Thermal and Material Flow Characteristics in Friction Stir Welding," Mater. Des., **77**, pp. 114–125.

[63] Chen, C. M., and Kovacevic, R., 2003, "Finite Element Modeling of Friction Stir Welding — Thermal and Thermomechanical Analysis," **43**, pp. 1319–1326.

[64] Zhang, H. W., Zhang, Z., and Chen, J. T., 2005, "The Finite Element Simulation of the Friction Stir Welding Process," Mater. Sci. Eng. A, **403**(1–2), pp. 340–348.

[65] Nandan, R., 2008, "Computational Modeling of Heat Transfer and Visco-Plastic Flow in Friction Stir Welding," (December), p. 196.

[66] Liu, X., Lan, S., and Ni, J., 2015, “Thermal Mechanical Modeling of the Plunge Stage During Friction-Stir Welding of Dissimilar Al 6061 to TRIP 780 Steel,” J. Manuf. Sci. Eng., **137**(5), p. 051017.

[67] Al-Badour, F., Merah, N., Shuaib, A., and Bazoune, A., 2013, “Coupled Eulerian Lagrangian Finite Element Modeling of Friction Stir Welding Processes,” J. Mater. Process. Technol., **213**(8), pp. 1433–1439.

[68] Sanjeev, N. K., and Ravikiran, B. ., “Application of Coupled Eulerian Lagrangian Approach in Finite Element Simulation of Friction Stir Welding.”

[69] Chen, K., Liu, X., and Ni, J., 2017, “Thermal-Mechanical Modeling on Friction Stir Spot Welding of Dissimilar Materials Based on Coupled Eulerian-Lagrangian Approach,” Int. J. Adv. Manuf. Technol., **91**(5–8), pp. 1697–1707.

[70] Stubblefield, G., Fraser, K. A., Canada, C., Jordon, J. B., and Allison, P. G., 2018, “Smoothed Particle Hydrodynamic Modeling of Additive Friction Stir Deposition Manufacturing of Aluminum Alloy 6061,” (July).

[71] Monaghan, J. J., 2005, “Smoothed Particle Hydrodynamics,” Reports Prog. Phys., **68**(8), pp. 1703–1759.

[72] Fraser, K. A., 2016, “Adaptive Thermal Boundary Conditions for Smoothed Particle Hydrodynamics Adaptive Thermal Boundary Conditions for Smoothed Particle Hydrodynamics,” (April).

[73] Bhojwani, S., “SMOOTHED PARTICLE HYDRODYNAMICS MODELING OF THE FRICTION STIR WELDING PROCESS.”

[74] Liu, M. B., and Liu, G. R., 2010, *Smoothed Particle Hydrodynamics (SPH): An Overview and Recent Developments*.

[75] Tartakovsky, A., Grant, G., Sun, X., and Khaleel, M., 2016, “Modeling of Friction Stir Welding (FSW) Process with Smooth Particle Hydrodynamics (SPH),” (724).

[76] Su, P., Gerlich, A., North, T. H., and Bendzsak, G. J., 2007, “Intermixing in Dissimilar Friction Stir Spot Welds,” Metall. Mater. Trans. A, **38**(3), pp. 584–595.

[77] Lacki, P., and Derlatka, A., 2016, “Experimental and Numerical Investigation of Aluminium Lap Joints Made by RFSSW,” Meccanica, **51**(2), pp. 455–462.

[78] Cox, C. D., Aguilar, J. R., Ballun, M. C., Strauss, A. M., and Cook, G. E., 2014, “The Application of a Pinless Tool in Friction Stir Spot Welding: An Experimental and Numerical Study,” Proc. Inst. Mech. Eng. Part D J. Automob. Eng., **228**(11), pp. 1359–1370.

[79] Miles, M., Karki, U., and Hovanski, Y., 2014, “Temperature and Material Flow Prediction in Friction-Stir Spot Welding of Advanced High-Strength Steel,” Jom, **66**(10), pp. 2130–2136.

[80] Assidi, M., Fourment, L., Guerdoux, S., and Nelson, T., 2010, “Friction Model for Friction Stir Welding Process Simulation: Calibrations from Welding Experiments,” Int. J. Mach. Tools Manuf., **50**(2), pp. 143–155.

[81] Veljić, D. M., Rakin, M. P., Perović, M. M., Medjo, B. I., Radaković, Z. J., Todorović, P. M., and Pavišić, M. N., 2013, “Heat Generation during Plunge Stage

in Friction Stir Welding," Therm. Sci., **17**(2), pp. 489–496.

[82] He, X. C., Pearson, I., and Young, K. W., 2007, "Finite Element Analysis of Self-Pierce Riveted Joints," Key Eng. Mater., **344**, pp. 663–668.

[83] Hamel, V., Roelandt, J. M., Gacel, J. N., and Schmit, F., 2000, "Finite Element Modeling of Clinch Forming with Automatic Remeshing," Comput. Struct., **77**(2), pp. 185–200.

[84] Pirondi, A., and Moroni, F., 2009, "Clinch-Bonded and Rivet-Bonded Hybrid Joints: Application of Damage Models for Simulation of Forming and Failure," J. Adhes. Sci. Technol., **23**(10–11), pp. 1547–1574.

[85] Bouchard, P. O., Laurent, T., and Tollier, L., 2008, "Numerical Modeling of Self-Pierce Riveting-From Riveting Process Modeling down to Structural Analysis," J. Mater. Process. Technol., **202**(1–3), pp. 290–300.

[86] Casalino, G., Rotondo, A., and Ludovico, A., 2008, "On the Numerical Modelling of the Multiphysics Self Piercing Riveting Process Based on the Finite Element Technique," Adv. Eng. Softw., **39**(9), pp. 787–795.

[87] Ma, Y., Li, Y., Hu, W., Lou, M., and Lin, Z., 2016, "Modeling of Friction Self-Piercing Riveting of Aluminum to Magnesium," J. Manuf. Sci. Eng., **138**(6), p. 061007.

[88] Porcaro, R., Hanssen, A. G., Aalberg, A., and Langseth, M., 2004, "Joining of Aluminium Using Self-Piercing Riveting: Testing, Modelling and Analysis," Int. J. Crashworthiness, **9**(2), pp. 141–154.

[89] Hoang, N. H., Hopperstad, O. S., Langseth, M., and Westermann, I., 2013, "Failure of Aluminium Self-Piercing Rivets: An Experimental and Numerical Study," Mater. Des., **49**, pp. 323–335.

[90] Mucha, J., 2014, "The Numerical Analysis of the Effect of the Joining Process Parameters on Self-Piercing Riveting Using the Solid Rivet," Arch. Civ. Mech. Eng., **14**(3), pp. 444–454.

[91] Grujicic, M., Snipes, J. S., and Ramaswami, S., 2015, "Process Modeling , Joint Virtual Testing and Construction of Joint Connectors for Mechanical Fastening by Flow-Drilling Screws."

[92] Ma, Y., Lou, M., Li, Y., and Lin, Z., 2018, "Modeling and Experimental Validation of Friction Self-Piercing Riveted Aluminum Alloy to Magnesium Alloy."

[93] Systemes, D., 2016, "Introduction to Abaqus About This Course," pp. 1–250.

[94] Johnson, G. R., and Cook, W. H., 1983, "A Constitutive Model and Data for Metals Subjected to Large Strains, High Strain Rates and High Temperatures," Proc. 7th Int. Symp. Ballist., **547**, pp. 541–547.

[95] Guo, Y. B., 2003, "An Integral Method to Determine the Mechanical Behavior of Materials in Metal Cutting," **142**, pp. 72–81.

[96] Hernández, C. A., Ferrer, V. H., Mancilla, J. E., and Martínez, L. C., 2017, "Three-Dimensional Numerical Modeling of the Friction Stir Welding of Dissimilar Steels," Int. J. Adv. Manuf. Technol., pp. 1567–1581.

[97] Hizli, İ. G., Bilen, A., Sezer, R., Yilmaz, E., Ertürk, S., and Arslan, C., 2017, *Investigating the Dissolution Characteristics of Strontium Sulfide*.

[98] Alcaraz, J., and Lorenzo, I., 2003, "Thermomechanical Analysis of a Chip Machining Process'," 2003 Users' Conf., pp. 1–10.

[99] D'Urso, G., and Giardini, C., 2016, "FEM Model for the Thermo-Mechanical Characterization of Friction Stir Spot Welded Joints," Int. J. Mater. Form., **9**(2), pp. 149–160.

[100] Absar, S., Ruszkiewicz, B. J., Skovron, J. D., Mears, L., Abke, T., Zhao, X., and Choi, H., 2018, "Temperature Measurement in Friction Element Welding Process with Micro Thin Film Thermocouples," Procedia Manuf., **26**, pp. 485–494.

[101] Hammelmüller, F., and Zehetner, C., "INCREASING NUMERICAL EFFICIENCY IN COUPLED EULERIAN- LAGRANGIAN METAL FORMING SIMULATIONS," pp. 727–733.

[102] Ajri, A., and Shin, Y. C., 2017, "Investigation on the Effects of Process Parameters on Defect Formation in Friction Stir Welded Samples Via Predictive Numerical Modeling and Experiments," **139**(November), pp. 1–10.

[103] Absar, S., Ruszkiewicz, B. J., Skovron, J. D., Mears, L., Abke, T., Zhao, X., and Choi, H., 2018, "ScienceDirect Temperature Measurement in Friction Element Welding Process with Micro Thin Film Thermocouples," **00**.